Article

Polyamine metabolite spermidine rejuvenates oocyte quality by enhancing mitophagy during female reproductive aging

Check for updates

Yu Zhang[1], Jie Bai[1], Zhaokang Cui[1], Yu Li[1], Qian Gao[2], Yilong Miao[1] & Bo Xiong ◉[1] ✉

Advanced age is a primary risk factor for female infertility due to reduced ovarian reserve and declining oocyte quality. However, as an important contributing factor, the role of metabolic regulation during reproductive aging is poorly understood. Here, we applied untargeted metabolomics to identify spermidine as a critical metabolite in ovaries to protect oocytes against aging. In particular, we found that the spermidine level was reduced in ovaries of aged mice and that supplementation with spermidine promoted follicle development, oocyte maturation, early embryonic development and female fertility of aged mice. By microtranscriptomic analysis, we further discovered that spermidine-induced recovery of oocyte quality was mediated by enhancement of mitophagy activity and mitochondrial function in aged mice, and this mechanism of action was conserved in porcine oocytes under oxidative stress. Altogether, our findings suggest that spermidine supplementation could represent a therapeutic strategy to ameliorate oocyte quality and reproductive outcome in cis-gender women and other persons trying to conceive at an advanced age. Future work is needed to test whether this approach can be safely and effectively translated to humans.

Fertility and reproductive lifespan in humans decrease dramatically with age, particularly after the mid-30s[1]. Approximately 10% of prospective female parents cannot achieve natural fertility under the age of 34 years, but this increases to 87% in those over 45 years of age[2]. Prospective female parents of advanced age may experience increased risk of infertility, spontaneous miscarriages, perinatal mortality and congenital anomaly[3]. Although assisted reproductive technologies can compensate for human suboptimal reproductive outcome to some extent, the success rate of assisted reproductive technology cycles declines with advanced age as well[4]. Female patients under 35 years of age undergoing

in vitro fertilization have a 41–43% rate of live births, whereas this drops to 1–2% when they reach the age of 44 years and above[5,6]. This tendency is mainly associated with age-related deterioration of ovarian reserve and oocyte quality, along with a higher aneuploidy rate[7]. Recent studies by us and others have reported that supplementation with nicotinamide mononucleotide (NMN) counteracts decaying fertility of aged female mice by improving oocyte quality[8–10]; however, more effective molecules and approaches still need to be discovered.

Polyamines, including putrescine, spermidine and spermine, are ubiquitously occurring polycations that are synthesized in almost every

[1]College of Animal Science and Technology, Nanjing Agricultural University, Nanjing, China. [2]College of Veterinary Medicine, Nanjing Agricultural University, Nanjing, China. ✉e-mail: xiongbo@njau.edu.cn

living cell and exist in many tissues, organs and organisms[11–14]. They bind and stabilize negatively charged molecules such as DNA, RNA, proteins and adenosine triphosphate (ATP) to take part in a diversity of physiological and pathophysiological processes[14]. Of these, spermidine is an intermediate polyamine compound that is synthesized from putrescine via the action of decarboxylated S-adenosyl methionine through spermidine synthase (SRM) and acts as a precursor of spermine by the action of spermine synthase (SMS)[11]. Spermidine was originally isolated from semen and is also found in most cells and tissues, including the ovary[15,16]. It participates in a wide range of cellular events, including regulation of transcription and translation, induction of oxidative stress, autophagy and apoptosis, and maintenance of genomic stability because of its anti-inflammatory activities, antioxidative properties, reinforced mitochondrial functions and enhanced proteostasis[17]. It has been reported that administration of spermidine prolongs lifespan in yeast, flies, worms and human immune cells through induction of autophagy[18,19]. In addition, dietary supplementation with spermidine suppressed age-induced memory impairment in *Drosophila*[20], prevented neurodegenerative diseases with TAR DNA-binding protein 43 (TDP-43) proteinopathies in mice[21] and exerted cardioprotective effects by reducing cardiac hypertrophy and a decline in diastolic function in old mice[22]. Although an increasing number of studies have been reported about the restorative role of spermidine for aging in somatic cells, the effect of spermidine on oocyte aging has not been clarified.

In the current study, we took advantage of untargeted metabolome analysis to discover that spermidine levels were reduced in ovaries of aged mice, and we found that supplementation with spermidine in vivo rejuvenated the quality of oocytes from aged mice by promoting their maturational competency, fertilization potential and embryonic development ability, thereby increasing animal fertility. Additionally, we determined that spermidine recovered mitophagy activity to inhibit apoptosis during oocyte aging by microtranscriptome analysis.

Results

The metabolome reveals reduced spermidine levels in ovaries of aged mice

To investigate how advanced age impacts metabolite changes in ovaries, we compared ovarian metabolome profiles between young and aged mice (Supplementary Data 1). Principal-component analysis revealed that five biological replicates clustered together in each group but were separated far from each other between young and aged samples (Fig. 1a). Heatmap analysis of differential metabolites showed that ovarian metabolome profiles were substantially altered in aged mice compared to those in young ones (Fig. 1b). In addition, a volcano plot displays the number of upregulated and downregulated metabolites in the aged group compared to the young counterpart (Fig. 1c). We further ranked the top ten pathways that were substantially altered in ovaries from aged mice compared to those of young ones by Kyoto Encyclopedia of Genes and Genomes (KEGG) enrichment analysis (Fig. 1d). Among them, one pathway was upregulated and nine pathways were downregulated as analyzed by differential abundance score (Fig. 1e). Notably, we found that spermidine, an intermediate polyamine compound that takes part in a variety of cellular processes, was present in both β-alanine metabolism and ATP-binding cassette (ABC) transporter pathways as a downregulated metabolite induced by aging (Fig. 1f,g). Also, the bar graph obtained from metabolome data showed that the level of spermidine was significantly reduced in ovaries of aged mice (Fig. 1h). Collectively, our metabolome data uncover the fact that spermidine is a critical metabolite that declines in ovaries of aged mice.

Spermidine improves ovarian development and female fertility of aged mice

To further validate whether aging would reduce the level of spermidine in ovaries, we performed an enzyme-linked immunosorbent assay-based spermidine-detection assay using mouse ovarian lysates. The enzyme-linked immunosorbent assay results showed that a substantial decrease in spermidine was observed in ovaries from aged mice compared to those from young controls (Fig. 2b). Strikingly, supplementation with spermidine by intraperitoneal injection remarkably increased the spermidine level in ovaries from aged mice and promoted the maturational rate of oocytes (Fig. 2a,b and Extended Data Fig. 1a), highlighting the potential role of spermidine in improving oocyte quality and female reproductive lifespan in animals of advanced age. We next evaluated ovarian development following spermidine supplementation in aged mice by hematoxylin and eosin staining of ovarian sections. We found that follicles at different developmental stages displayed normal morphology in ovaries from young mice (Fig. 2c and Extended Data Fig. 1b). On the contrary, a large number of degenerated follicles were present in ovaries of aged mice but were partially recovered in ovaries of spermidine-supplemented mice as assessed by terminal deoxynucleotidyl transferase dUTP nick end labeling (TUNEL) staining (Fig. 2e,f). Consistently, quantification of follicle number at different developmental stages revealed that spermidine supplementation increased the number of pre-antral and antral follicles in ovaries of aged mice (Fig. 2d). Consequently, the fertility test showed that the litter size of female mice was considerably lowered by aging, whereas it was restored to some degree after spermidine supplementation (Fig. 2g,h). Altogether, these data suggest that replenishment of spermidine is a feasible strategy to improve oocyte and ovarian development as well as female fecundity of aged animals.

Spermidine enhances the in vivo maturation competency of oocytes from aged mice

As the development of ovaries from aged mice was restored by supplementation with spermidine, we then assessed its effects on oocyte quality. After superovulation, we collected oocytes for counting and evaluating morphology. We found that the number of ovulated oocytes and their maturational rate as judged by extrusion of the first polar body (PB1) from aged mice was dramatically lower than that in the young ones, but the incidence of fragmentation was significantly increased (Fig. 3a–d). By contrast, supplementation with spermidine rescued the defects in the quantity and quality of oocytes from aged mice (Fig. 3a–d).

Given that the occurrence of aneuploidy is one of the key hallmarks for aging-induced low-quality oocytes, spindle–chromosome structure and chromosome number were further examined. By immunofluorescent staining and confocal imaging, we observed that barrel-like spindle apparatuses with well-aligned chromosomes were present in most oocytes from young mice, while various morphology-aberrant spindles with misaligned chromosomes were found in oocytes from aged mice (Fig. 3e). Notably, some spindle–chromosome abnormalities in oocytes from aged mice were restored following spermidine supplementation (Fig. 3e). Quantification data also showed that the proportions of abnormal spindles and misaligned chromosomes were considerably higher in oocytes from aged mice than those from young ones but were reduced in oocytes from spermidine-supplemented mice (Fig. 3f,g). In line with these observations, the results of chromosome spreading and counting showed that the frequency of aneuploidy as assessed by more than or less than 20 univalents remarkably grew in oocytes from aged mice in comparison with that of young controls, whereas it declined with spermidine supplementation (Fig. 3h,i). Collectively, our observations indicate that spermidine could ameliorate aging-induced meiotic defects during oocyte nuclear maturation.

Spermidine recovers the fertilization capacity and early embryonic development potential of oocytes from aged mice

Aside from nuclear maturation, cytoplasmic maturation is another pivotal process that determines the quality of oocytes and is highly related to subsequent fertilization and embryonic development.
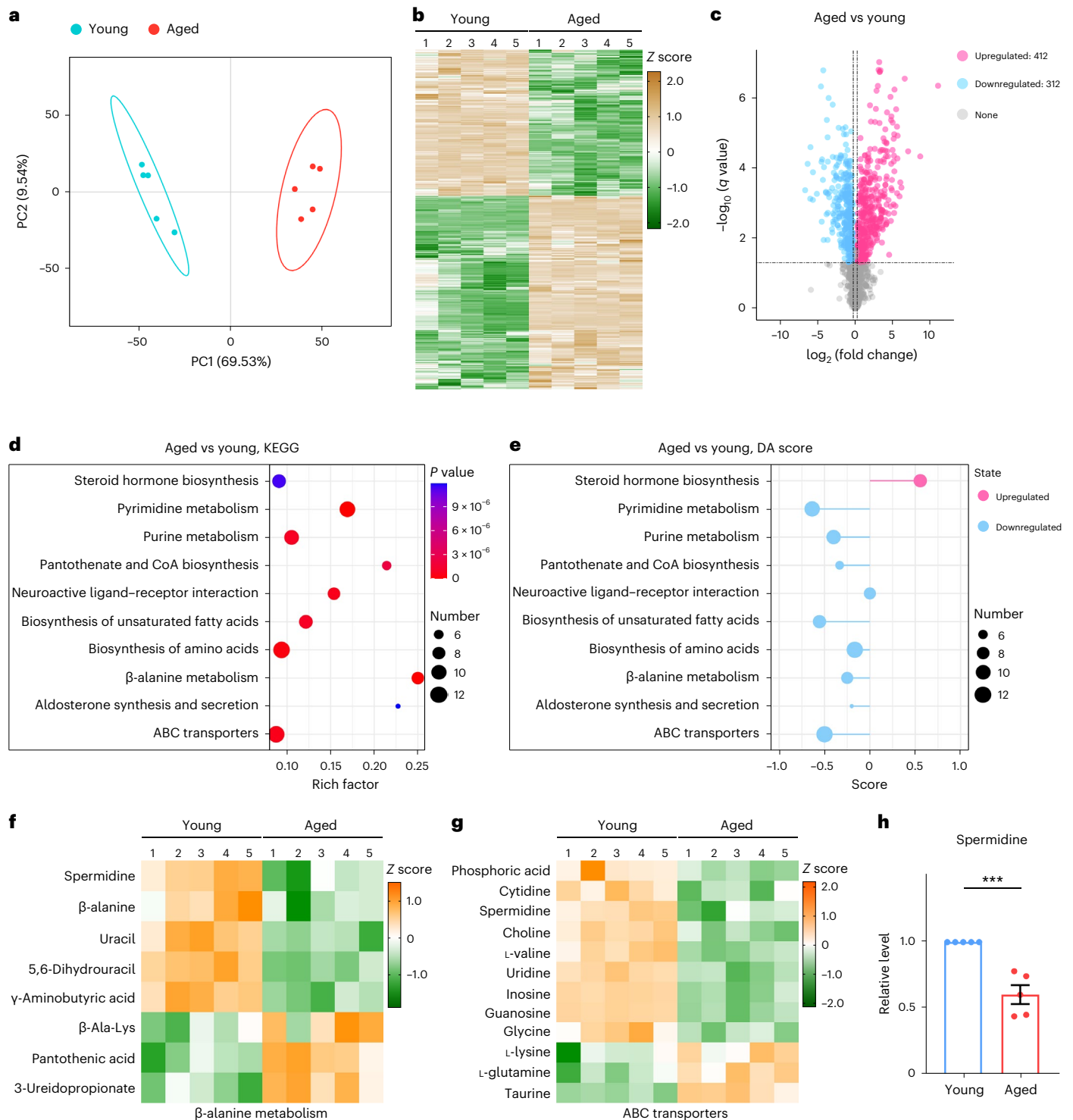
Fig. 1 | Metabolome profiling of ovaries in aged mice. a, Principal-component (PC) analysis of samples from ovaries of young and aged mice. Blue circles represent samples from the young group, and red circles represent samples from the aged group. **b**, Heatmap illustration shows differential metabolites in ovaries from young versus aged mice. **c**, Volcano plot displays differential metabolites (upregulated, red; downregulated, blue) in ovaries from aged mice compared to those from young ones. **d**, KEGG enrichment analysis of differential metabolites in ovaries from aged mice compared to those from young controls. CoA, coenzyme A. **e**, Differential abundance (DA) score analysis of differential metabolites (upregulated, red; downregulated, blue) in ovaries from aged mice compared to those from young ones. **f**, Heatmap illustration displays differential metabolites in the β-alanine metabolism pathway in ovaries from young and aged mice. **g**, Heatmap illustration displays differential metabolites in the ABC transporter pathway in ovaries from young and aged mice. **h**, Metabolome data show levels of spermidine in ovaries from young and aged mice. ***$P = 0.0005$. Data are expressed as mean percentage (mean ± s.e.m.) of five biologically independent samples. Statistical significance was determined by two-tailed unpaired t-test.

We thus investigated the dynamics of cortical granules (CGs) and mitochondria, two critical indicators of oocyte cytoplasmic maturation. By fluorescent imaging and intensity measurement, we found that the signals of CGs on the subcortical region of oocytes as shown by lens culinaris agglutinin, fluorescein (LCA–FITC) staining were prominently reduced in oocytes from aged mice compared to those in young ones and were effectively restored in the spermidine-supplemented group (Fig. 4a,b). Consistent with this observation, spermidine supplementation also maintained the level of ovastacin, a key component of CGs associated with sperm-binding ability, in the subcortex of oocytes from aged mice (Extended Data Fig. 2a,b). Furthermore, staining of mitochondria with MitoTracker Red revealed that mitochondria were distributed evenly in the cytoplasm with accumulation around the spindle in oocytes from young mice (Fig. 4c,d and Extended Data Fig. 2c). However, aging compromised this distribution pattern of mitochondria, showing faded signals in the cytoplasm and loss of aggregation around chromosomes, which was rescued by spermidine supplementation to some extent (Fig. 4c,d).

Because the anomalous dynamics of CGs and ovastacin may impair the sperm-binding ability of oocytes, we next tested this in the sperm–oocyte binding assay. Counting of sperm head binding to the zona pellucida (ZP) of oocytes indicated that oocytes from young mice supported robust binding of an abundance of sperm before fertilization but lost it after fertilization (Fig. 4e,f). By striking contrast, the number of sperm binding to oocytes from aged mice was remarkably lower even before fertilization, indicative of the weakened sperm-binding ability caused by aging (Fig. 4e,f). Similarly, spermidine supplementation increased the number of sperm binding to oocytes from aged mice. In the meantime, we also demonstrated that spermidine supplementation restored rates of in vitro fertilization and blastocyst formation that were markedly decreased in oocytes from aged mice (Fig. 4g–i). Therefore, our results imply that spermidine strengthens the fertilization capacity and embryonic development potential of oocytes from aged mice by promoting their cytoplasmic maturation.

To further verity the beneficial action of spermidine on oocytes from aged mice, dietary supplementation with spermidine in drinking water was performed. We found that the quality of oocytes from aged mice including maturation competency, spindle–chromosome structure, chromosome euploidy, fertilization capacity and early embryonic development potential was prominently improved by dietary supplementation with spermidine (Extended Data Fig. 3), demonstrating that spermidine supplementation by different administration methods enhances the quality of oocytes impaired by aging.

Spermidine boosts in vitro maturation of oocytes from aged mice

Because supplementation with spermidine could enhance in vivo maturation of oocytes from aged mice, we further asked whether it had a favorable effect on in vitro maturation by supplementing spermidine at different concentrations in the culture medium to observe PB1 extrusion in oocytes. Statistical data indicated that supplementation with 50 µM spermidine significantly recovered PB1 extrusion after in vitro maturation of germinal vesicle (GV) oocytes from aged mice (Fig. 5a,b and Extended Data Fig. 4a). In addition, in most oocytes from young mice, the spindle apparatus normally assembled around well-aligned chromosomes at metaphase I, with the correct attachment of kinetochores on chromosomes by microtubule fibers (Fig. 5c–g). While a higher percentage of disorganized spindles, misaligned chromosomes and improper attachment of kinetochores and microtubules was present in oocytes from aged mice, which was considerably decreased by spermidine supplementation (Fig. 5c–g). Accordingly, spindle–chromosome structure at metaphase II after in vitro maturation was also disrupted by aging and restored following spermidine supplementation (Extended Data Fig. 4b–d). As a result, spermidine supplementation reduced the occurrence of aneuploidy from ~40% to ~20% in oocytes at metaphase II from aged mice (Fig. 5h,i). In conclusion, we demonstrate that supplementation with spermidine during in vitro maturation also rejuvenated the quality of oocytes from aged mice.

Microtranscriptomic analysis reveals regulatory pathways involved in spermidine effects on oocytes from aged mice

To gain insight into potential mechanisms regarding how spermidine improves the quality of oocytes from aged mice, microtranscriptomics was carried out to compare changes in transcript levels (Supplementary Data 2). Heatmap analysis showed remarkably different transcriptomic profiling between oocytes from young and aged mice, and the profile was partially restored in oocytes from spermidine-supplemented mice (Fig. 6a). Volcano plots and fold-change graphs further revealed that 516 upregulated and 307 downregulated transcripts were present in oocytes from aged mice compared to those from young ones (Fig. 6b and Extended Data Fig. 5a); furthermore, 122 upregulated and 136 downregulated transcripts were observed in oocytes from spermidine-supplemented mice compared to those from aged ones (Fig. 6c and Extended Data Fig. 5b). Additionally, a Venn diagram presents the overlapping differentially expressed genes (DEGs) between these two groups (Extended Data Fig. 5c). There were also some DEGs between oocytes from spermidine-supplemented mice compared to those from young ones (Extended Data Fig. 5d). By performing KEGG analysis, we noticed that transcripts of DEGs were enriched in pathways related to oxidative phosphorylation and autophagy in oocytes from aged mice in comparison with those from young counterparts, which was rescued by spermidine supplementation (Fig. 6d,e). KEGG network analysis also indicated that these DEGs in the autophagy and mitophagy pathways might be associated with the apoptosis pathway (Extended Data Fig. 5e,f). In addition, gene ontology (GO) analyses in both oocytes from aged mice compared to young controls and oocytes from spermidine-supplemented mice compared to those from aged ones showed that DEGs were enriched in biological processes such as apoptosis, cell cycle and mitochondrial organization (Fig. 6f,g). Therefore, from the above observations, we hypothesize that the improvement in oocyte quality from aged mice induced by spermidine supplementation might be mediated through autophagy and mitochondrial functions.

Fig. 2 | Effects of spermidine supplementation on the ovarian spermidine level, follicle development and female fertility in aged mice. a, A timeline scheme for spermidine (Spd) supplementation, hormone priming and subsequent analyses. hCG, human chorionic gonadotropin; PMSG, pregnant mare serum gonadotropin; MII, metaphase II. **b**, Spermidine levels were measured in the lysates of ovaries from young mice ($n = 60$), aged mice ($n = 36$) and aged mice supplemented with spermidine (Spd + aged) ($n = 36$). ***$P = 0.0001$, *$P = 0.0465$. **c**, Representative images of ovarian sections from young, aged and Spd + aged mice. Scale bars, a′, 300 µm; b′, 150 µm. **d**, Numbers of follicles at different developmental stages were counted in each ovarian section from young ($n = 6$), aged ($n = 6$) and Spd + aged ($n = 6$) mice. ****$P < 0.0001$, $P = 0.6912$; ****$P < 0.0001$, $P = 0.9060$; ****$P < 0.0001$, $P = 0.7925$; ****$P < 0.0001$, $P = 0.0404$; ***$P = 0.0005$, *$P = 0.0224$. PmF, primordial follicle; PF, primary follicle; SF, secondary follicle; PAF, pre-antral follicle; AF, antral follicle; NS, not significant. **e**, Representative images of degenerated follicles stained with TUNEL. Scale bars, 250 µm and 100 µm. **f**, The percentage of TUNEL-positive follicles was quantified in young ($n = 6$), aged ($n = 6$) and Spd + aged ($n = 6$) mice. **$P = 0.0012$, *$P = 0.0242$. **g**, Representative images of pups delivered by young, aged and Spd + aged mice. Scale bar, 2 cm. **h**, The litter size of young ($n = 9$), aged ($n = 9$) and Spd + aged ($n = 9$) female mice was quantified after mating with young male mice. ****$P < 0.0001$, **$P = 0.003$. Data in **b,d,f,h** are expressed as mean percentage (mean ± s.e.m.) of at least three independent experiments. Statistical significance was determined by two-tailed unpaired t-test.
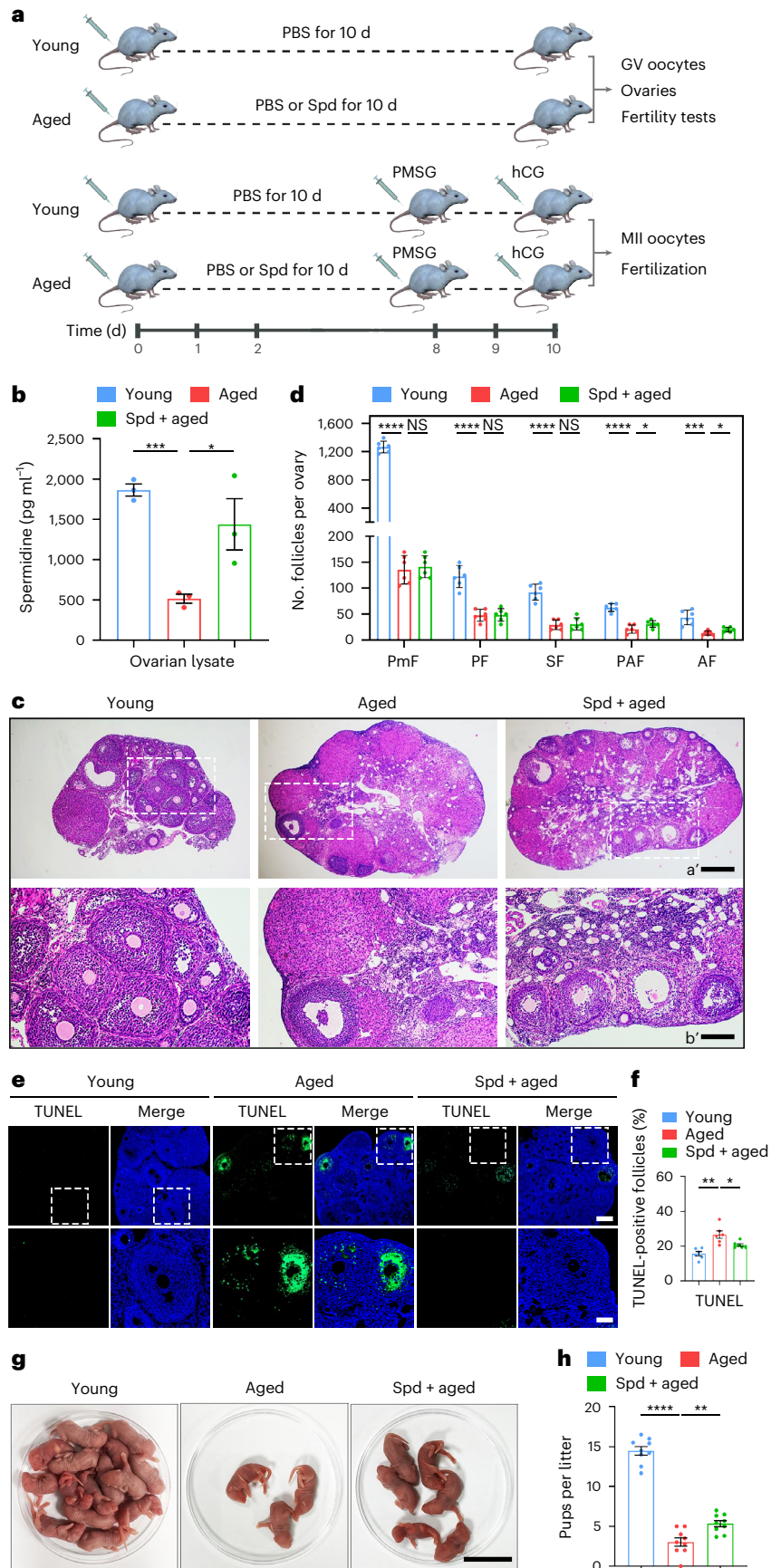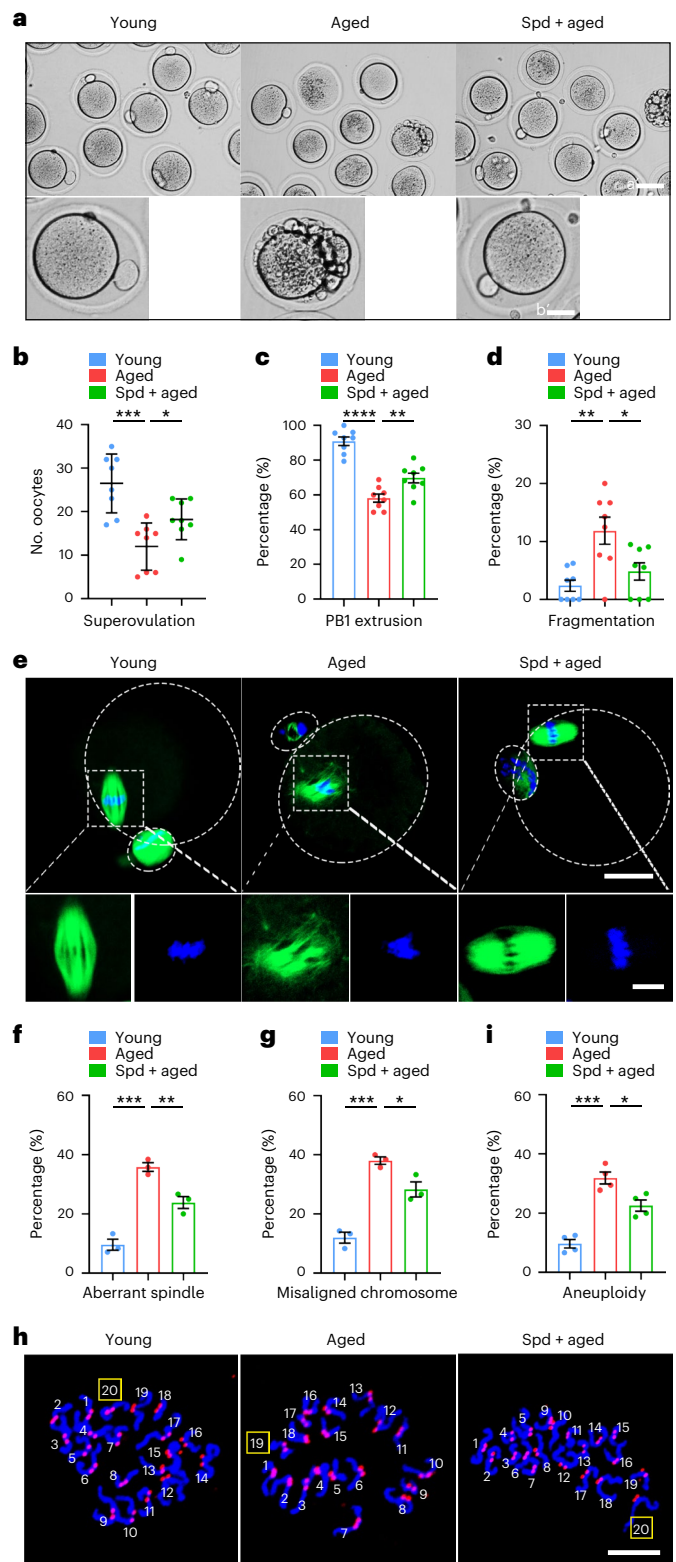

Spermidine restores autophagy in oocytes from aged mice

A heatmap of DEGs enriched in the autophagy pathway indicated that spermidine supplementation to some degree recovered transcript levels of 26 genes in oocytes from aged mice (Fig. 7a). We randomly selected four of them to verify their mRNA levels in each group of oocytes by PCR with reverse transcription (RT–PCR), and the results were consistent with the RNA-seq data (Fig. 7b,c). As autophagy is featured by the formation of autophagosomes that fuse with lysosomes to form autolysosomes, we next examined autophagy by staining for the autophagosome marker microtubule-associated protein 1A or 1B light chain 3 (LC3). Fluorescence imaging and quantification results illustrated that a great number of LC3 signals with many large foci were present in oocytes from young mice (Fig. 7d,e). By striking contrast, aging reduced both amount and size of LC3 foci, and this was recovered by spermidine supplementation (Fig. 7d,e). Furthermore, we validated autolysosome formation by double staining with anti-LC3 antibody and LysoTracker Green. A colocalization pattern of LC3 foci and lysosome vesicles was observed in oocytes from young and spermidine-supplemented mice but was lost in those from aged ones (Fig. 7f). Quantitatively, both Pearson's correlation coefficient (PCC) and Mander's correlation coefficient (MCC) analyses showed that the relationship between signals from LC3 and lysosomes became much weaker in oocytes from aged mice compared to that from young ones, and it was strengthened by spermidine supplementation (Fig. 7g and Extended Data Fig. 6a,b). Thus, our data indicate that spermidine is able to elevate autophagy in oocytes from aged mice.

Spermidine enhances mitophagy and mitochondrial function in oocytes from aged mice

Mitophagy is a specialized form of autophagy that mediates the removal of dysfunctional mitochondria to maintain both mitochondrial quantity and quality. Taking advantage of our RNA-seq data, we displayed mRNA levels of 11 DEGs related to the mitophagy pathway in a heatmap, indicating that spermidine supplementation rescued the change in transcript levels of these DEGs in oocytes from aged mice (Fig. 8a). Also, RT–PCR results of two selected DEGs further confirmed the transcriptomic data (Fig. 8b,c). We then tested the formation of mitophagosomes by double staining for voltage-dependent anion channel 1 (VDAC1), a pivotal protein required for PTEN-induced kinase 1 (PINK1)–parkin-mediated mitophagy, and LC3. PCC and MCC analyses based on the fluorescence signals demonstrated that most VDAC1 signals colocalized with LC3 foci in the cytoplasm of oocytes from

young mice, but only a few VDAC1 signals colocalized with LC3 foci in oocytes from aged mice (Fig. 8d,e and Extended Data Fig. 6c,d). On the contrary, spermidine dramatically promoted colocalization of VDAC1 and LC3 signals in oocytes from aged mice (Fig. 8d,e and Extended Data Fig. 6c,d), implying that the impaired mitophagosomes caused by aging in oocytes can be restored after spermidine supplementation. In addition, the formation of mitolysosomes in each group of oocytes was assessed by double staining with MitoTracker Red and LysoTracker
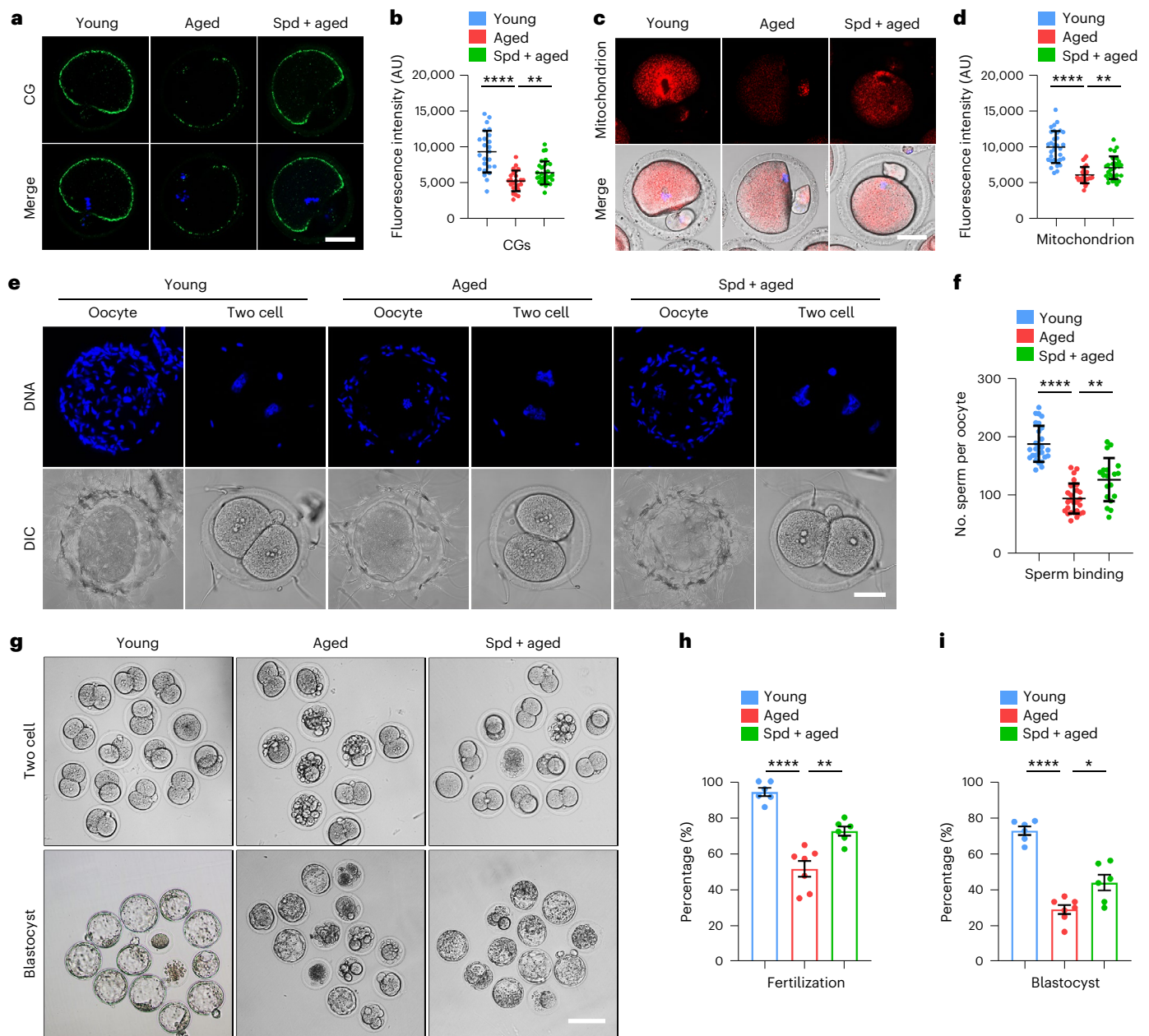

Fig. 3 | Effects of spermidine supplementation on in vivo maturation of oocytes from aged mice. a, Representative images of in vivo matured oocytes collected from young, aged and Spd + aged mice. Scale bars, a′, 50 μm; b′, 30 μm. **b,** The number of ovulated oocytes was counted in young (n = 8), aged (n = 8) and Spd + aged (n = 8) mice. ***P = 0.0003, *P = 0.0272. **c,** The percentage of PB1 extrusion was quantified in oocytes from young (n = 212), aged (n = 96) and Spd + aged (n = 146) mice. ****P < 0.0001, **P = 0.0065. **d,** The proportion of fragmentation was quantified in oocytes from young (n = 212), aged (n = 96) and Spd + aged (n = 146) mice. **P = 0.002, *P = 0.0232. **e,** Representative images of spindle morphology and chromosome alignment in oocytes at the metaphase II stage from young, aged and Spd + aged mice. Scale bars, 20 μm and 10 μm. **f,** The percentage of aberrant spindles was quantified in oocytes at metaphase II from young (n = 41), aged (n = 42) and Spd + aged (n = 46) mice. ***P = 0.0004, **P = 0.0087. **g,** The percentage of misaligned chromosomes was quantified in oocytes at metaphase II from young (n = 41), aged (n = 42) and Spd + aged (n = 46) mice. ***P = 0.0003, *P = 0.0266. **h,** Representative images of chromosome numbers in oocytes at metaphase II from young, aged and Spd + aged mice. Scale bar, 5 μm. **i,** The proportion of aneuploidy was quantified in oocytes at metaphase II from young (n = 61), aged (n = 69) and Spd + aged (n = 62) mice. ***P = 0.0001, *P = 0.0162. Data in **b** are expressed as mean value (mean ± s.d.) and data in **c,d,f,g,i** are expressed as mean percentage (mean ± s.e.m.) of at least three independent experiments. Statistical significance was determined by two-tailed unpaired t-test.

Fig. 4 | Effects of spermidine supplementation on the fertilization capacity and embryonic development potential of oocytes from aged mice.
a, Representative images of CG distribution in oocytes at metaphase II from young, aged and Spd + aged mice. Scale bar, 30 µm. **b**, The fluorescence intensity of CG signals was measured in oocytes at metaphase II from young ($n = 24$), aged ($n = 24$) and Spd + aged ($n = 30$) mice. ****$P < 0.0001$, **$P = 0.0085$. **c**, Representative images of mitochondrial distribution in oocytes at metaphase II from young, aged and Spd + aged mice. Scale bar, 30 µm. **d**, The fluorescence intensity of mitochondrial signals was quantified in oocytes at metaphase II from young ($n = 32$), aged ($n = 29$) and Spd + aged ($n = 30$) mice. ****$P < 0.0001$, **$P = 0.0059$. **e**, Representative images of sperm binding to the ZP surrounding oocytes at metaphase II from young, aged and Spd + aged mice. DIC, differential interference contrast. Scale bar, 30 µm. **f**, The numbers of sperm binding to the ZP of oocytes at metaphase II from young ($n = 27$), aged ($n = 27$) and Spd + aged ($n = 19$) mice were counted. ****$P < 0.0001$, **$P = 0.0011$. **g**, Representative images of two-cell embryos and blastocysts developed from in vivo fertilized oocytes from young, aged and Spd + aged mice. Scale bar, 120 µm. **h**, The fertilization rate was quantified in young ($n = 147$), aged ($n = 134$) and Spd + aged ($n = 120$) groups. ****$P < 0.0001$, **$P = 0.0022$. **i**, The proportion of blastocyst formation was quantified in young ($n = 147$), aged ($n = 134$) and Spd + aged ($n = 120$) groups. ****$P < 0.0001$, *$P = 0.0104$. Data in **b,d,f** are expressed as mean value (mean ± s.d.) and data in **h,i** are expressed as mean percentage (mean ± s.e.m.) of at least three independent experiments. Statistical significance was determined by two-tailed unpaired t-test.

Green. Similarly, colocalization of mitochondria and lysosomes was compromised by aging in oocytes and could be recovered by supplementation with spermidine as evaluated by PCC and MCC analyses of fluorescence signals (Fig. 8f,g and Extended Data Fig. 6e,f). These findings illustrate that spermidine reinforces mitophagy activity in oocytes from aged mice.

To investigate whether mitophagy enhancement would strengthen mitochondrial function, we detected mitochondrial membrane potential ($\Delta\Psi_m$) by 5,5′,6,6′-tetrachloro-1,1′,3,3′-tetraethylbenzi midazolylcarbocyanine iodide (JC-1) staining. The ratio of J-aggregates at high $\Delta\Psi_m$ to JC-1 monomers at low $\Delta\Psi_m$ was found to be high in oocytes from young mice but decreased in those from aged mice
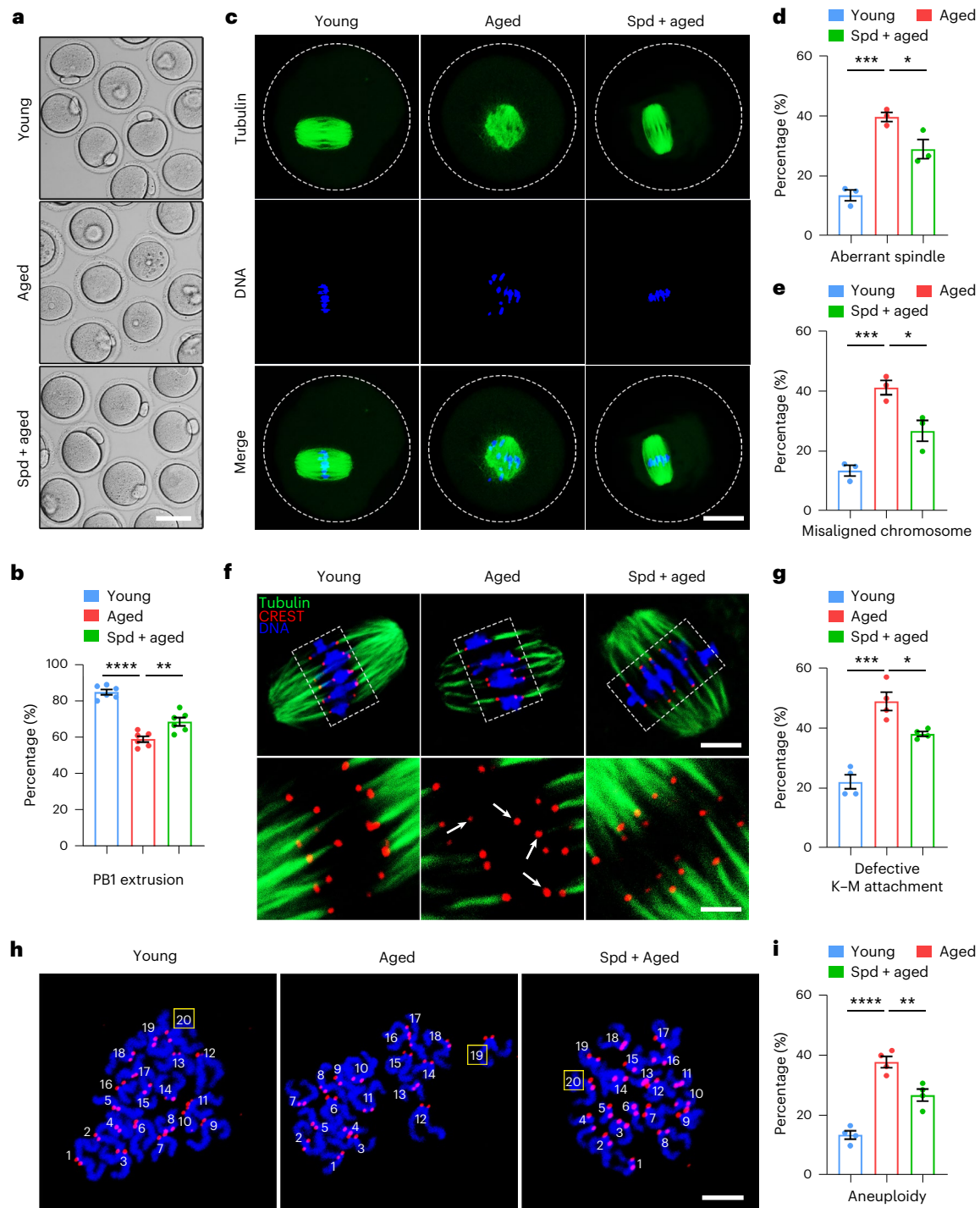
Fig. 5 | Effects of spermidine supplementation on in vitro maturation of oocytes from aged mice. a, Representative images of in vitro matured oocytes cultured from GV oocytes from young, aged and Spd + aged mice. Scale bar, 80 μm. **b**, The percentage of PB1 extrusion was quantified in oocytes from young ($n = 177$), aged ($n = 168$) and Spd + aged ($n = 165$) mice after in vitro maturation for 14 h. ****$P < 0.0001$, **$P = 0.0064$. **c**, Representative images of spindle morphology and chromosome alignment in oocytes at the metaphase I stage from young, aged and Spd + aged mice. Scale bar, 20 μm. **d**, The percentage of aberrant spindles was quantified in oocytes at metaphase I from young ($n = 59$), aged ($n = 58$) and Spd + aged ($n = 48$) mice. ***$P = 0.0004$, *$P = 0.0394$. **e**, The percentage of misaligned chromosomes was quantified in oocytes at metaphase I from young ($n = 59$), aged ($n = 58$) and Spd + aged ($n = 48$) mice. ***$P = 0.0008$, *$P = 0.0269$. **f**, Representative images of kinetochore–microtubule attachment

in oocytes at metaphase I from young, aged and Spd + aged mice. CREST, calcinosis, Raynaud's phenomenon, esophageal dysmotility, sclerodactyly, and telangiectasia. Scale bars, 10 μm, 5 μm. **g**, The percentage of defective kinetochore–microtubule (K–M) attachment was quantified in oocytes at metaphase I from young ($n = 45$), aged ($n = 43$) and Spd + aged ($n = 47$) mice. ***$P = 0.0004$, *$P = 0.0141$. **h**, Representative images of chromosome numbers in oocytes at metaphase II from young, aged and Spd + aged mice. Scale bar, 5 μm. **i**, The percentage of aneuploidy was quantified in oocytes at metaphase II from young ($n = 51$), aged ($n = 53$) and Spd + aged ($n = 56$) mice. ****$P < 0.0001$, **$P = 0.007$. Data in **b**,**d**,**e**,**g**,**i** are expressed as mean percentage (mean ± s.e.m.) of at least three independent experiments. Statistical significance was determined by two-tailed unpaired t-test.
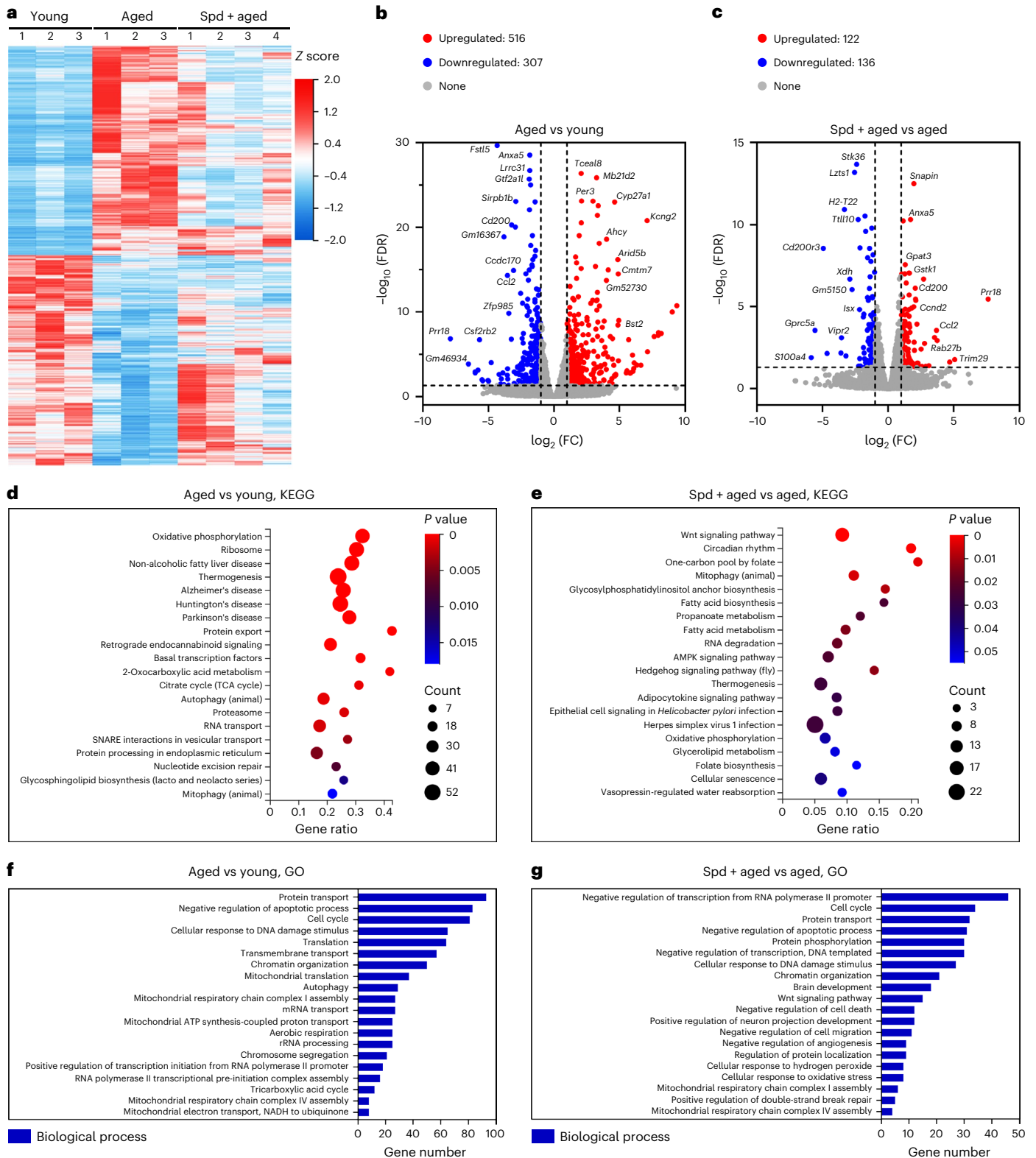
Fig. 6 | Effects of spermidine supplementation on the transcriptome level of oocytes from aged mice. a, Heatmap illustration shows total DEGs in oocytes from young, aged and Spd + aged mice. **b**, Volcano plot displays DEGs (upregulated, red; downregulated, blue) in oocytes from aged mice compared to those from young controls. Several highly different DEGs are listed. FC, fold change; FDR, false discovery rate. **c**, Volcano plot shows DEGs (upregulated, red; downregulated, blue) in oocytes from Spd + aged mice compared to those from aged ones. Several highly different DEGs are listed. **d**, KEGG analysis of DEGs in oocytes from aged mice compared to young controls. TCA, tricarboxylic acid. SNARE, soluble N-ethylmaleimide-sensitive factor protein attachment protein receptor. **e**, KEGG of DEGs in oocytes from Spd + aged mice compared to those from aged ones. AMPK, AMP-activated protein kinase. **f**, GO analysis of DEGs in oocytes from aged mice compared to those from young controls. **g**, GO analysis of DEGs in oocytes from Spd + aged mice compared to those from aged ones.
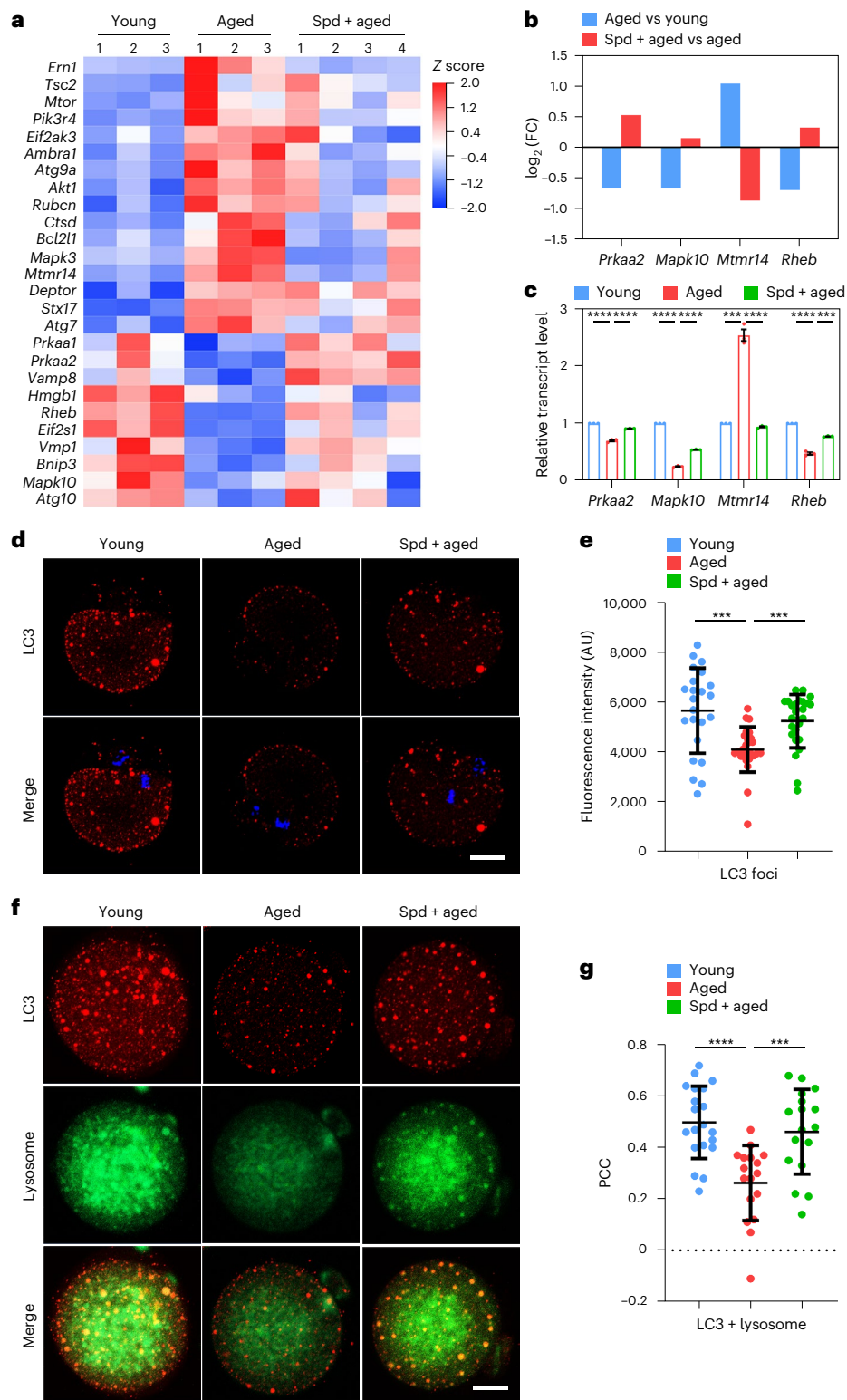
Fig. 7 | Effects of spermidine supplementation on autophagy in oocytes from aged mice. a, Heatmap illustration shows DEGs in the autophagy pathway in oocytes from young, aged and Spd + aged mice. **b**, RNA-seq results of selected DEGs in the autophagy pathway in oocytes from aged mice compared to those from young controls and in oocytes from Spd + aged mice compared to those from aged ones. **c**, Validation of RNA-seq data by quantitative RT–PCR in oocytes from young (*n* = 30), aged (*n* = 30) and Spd + aged (*n* = 30) mice. ****P < 0.0001, ****P < 0.0001; ****P < 0.0001, ****P < 0.0001; ***P = 0.0001, ****P < 0.0001; ****P < 0.0001, ***P = 0.0002. **d**, Representative images of autophagosomes stained with anti-LC3 antibody in oocytes at metaphase II from young, aged and Spd + aged mice. Scale bar, 20 μm. **e**, The fluorescence intensity of signals from

LC3 was quantified in oocytes at metaphase II from young (*n* = 23), aged (*n* = 26) and Spd + aged (*n* = 25) mice. ***P = 0.0002, ***P = 0.0002. **f**, Representative images of autolysosomes co-stained with anti-LC3 antibody and LysoTracker Green in oocytes at metaphase II from young, aged and Spd + aged mice. Scale bar, 20 μm. **g**, PCC of signals from LC3 and lysosomes was calculated in oocytes at metaphase II from young (*n* = 20), aged (*n* = 17) and Spd + aged (*n* = 17) mice. ****P < 0.0001, ***P = 0.0007. Data in **c** are expressed as mean value (mean ± s.e.m.) and data in **e,g** are expressed in mean value (mean ± s.d.) of at least three independent experiments. Statistical significance was determined by two-tailed unpaired *t*-test.
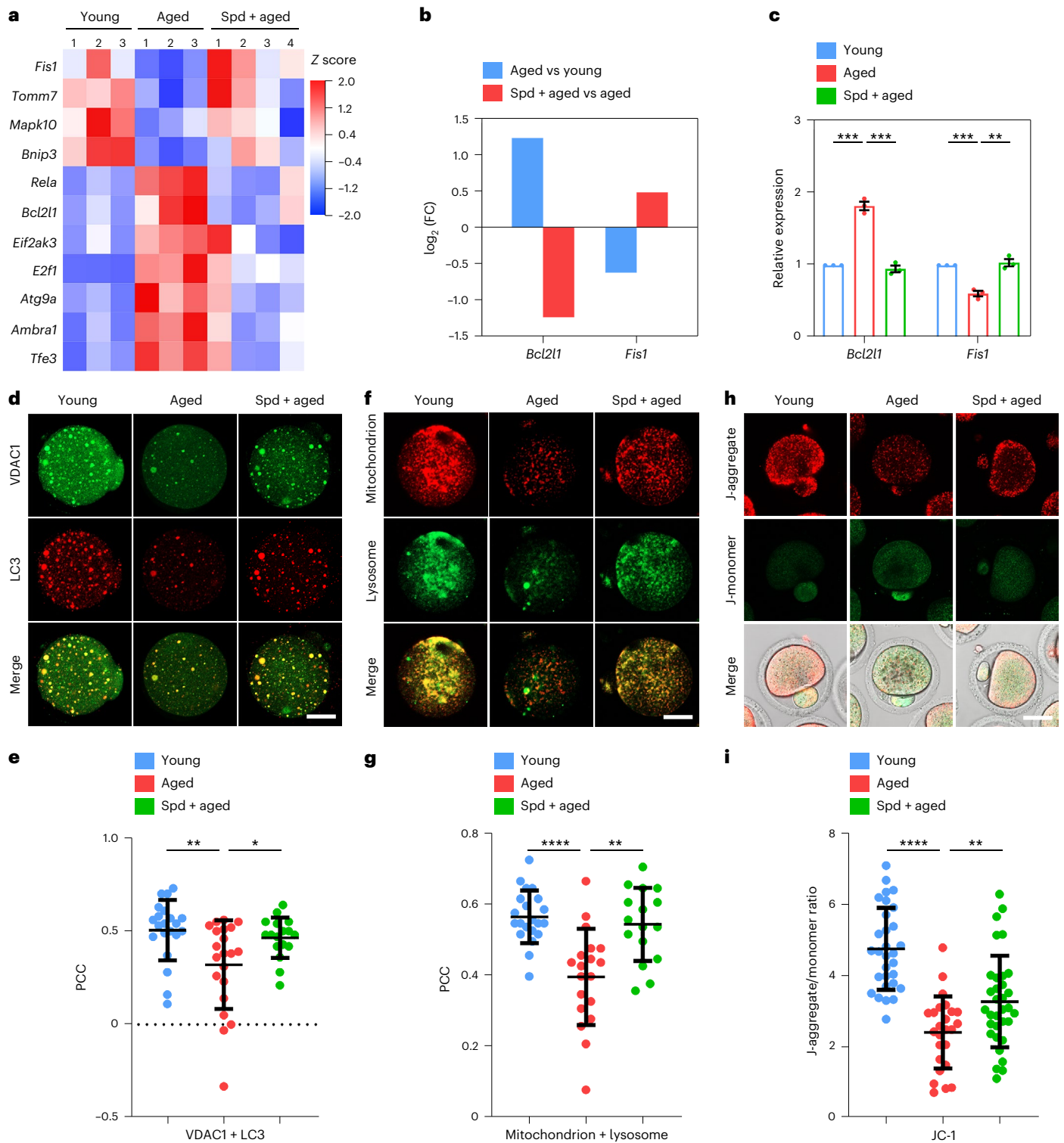
Fig. 8 | Effects of spermidine supplementation on mitophagy activity of oocytes from aged mice. a, Heatmap illustration displays DEGs in the mitophagy pathway in oocytes from young, aged and Spd + aged mice. **b**, RNA-seq results of selected DEGs in the mitophagy pathway in oocytes from aged mice compared to those from young controls and in oocytes from Spd + aged mice compared to those from aged mice. **c**, Validation of RNA-seq data by quantitative RT–PCR in oocytes from young (n = 30), aged (n = 30) and Spd + aged (n = 30) mice. ***P = 0.0001, ***P = 0.0003; ***P = 0.0006, **P = 0.0027. **d**, Representative images of mitophagosomes co-stained with anti-VDAC1 and anti-LC3 antibodies in oocytes at metaphase II from young, aged and Spd + aged mice. Scale bar, 20 μm. **e**, The PCC of VDAC1 and LC3 signals was calculated in oocytes at metaphase II from young (n = 21), aged (n = 21) and Spd + aged (n = 17) mice. **P = 0.0052, *P = 0.0212. **f**, Representative images of

mitolysosomes co-stained with MitoTracker Red and LysoTracker Green in oocytes at metaphase II from young, aged and Spd + aged mice. Scale bar, 20 μm. **g**, The PCC of mitochondrion and lysosome signals was calculated in oocytes at metaphase II from young (n = 21), aged (n = 19) and Spd + aged (n = 16) mice. ****P < 0.0001, **P = 0.0011. **h**, Representative images of mitochondrial membrane potential ($\Delta\Psi_m$) levels as assessed by JC-1 staining in oocytes at metaphase II from young, aged and Spd + aged mice (red, high $\Delta\Psi_m$; green, low $\Delta\Psi_m$). Scale bar, 20 μm. **i**, The ratio of red to green fluorescence intensity was quantified in oocytes at metaphase II from young (n = 30), aged (n = 25) and Spd + aged (n = 33) mice. ****P < 0.0001, **P = 0.0074. Data in **c** are expressed as mean value (mean ± s.e.m.) and data in **e,g,i** (mean ± s.d.) of at least three independent experiments. Statistical significance was determined by two-tailed unpaired t-test.

(Fig. 8h,i). By comparison, spermidine supplementation substantially elevated the $\Delta\Psi_m$ level in oocytes from aged mice (Fig. 8h,i), indicative of improvement in mitochondrial function. In line with previous studies by us and others[9,23,24], we observed that mitochondrial dysfunction in oocytes caused by aging produced excessive reactive oxygen species (ROS), accumulated DNA damage and high incidence of apoptosis as evaluated by fluorescence imaging and intensity quantification (Extended Data Fig. 7). As expected, spermidine supplementation effectively reduced the levels of ROS and DNA damage, thus inhibiting apoptosis (Extended Data Fig. 7). In sum, we demonstrate that spermidine strengthens mitochondrial function through activation of mitophagy.

Inhibition of mitophagy activity interferes with the spermidine-enhanced quality of oocytes from aged mice

To further validate that the favorable effects of spermidine on oocytes from aged mice were mediated by mitophagy, we cultured oocytes from aged mice in maturation medium containing both spermidine and the mitophagy inhibitor Mdivi-1 to assess oocyte maturation. The concentration of Mdivi-1 was determined by observing the rate of PB1 extrusion and the intensity of LC3 signals in oocytes from young mice (Extended Data Fig. 8a–c). Notably, in the presence of Mdivi-1, the maturation rate of oocytes from aged mice treated with spermidine as evaluated by PB1 extrusion was even lower than that of aged ones (Extended Data Fig. 8d). Furthermore, measurement of fluorescence intensity of LC3 signals indicated that Mdivi-1 treatment also impaired spermidine-induced mitophagy recovery in oocytes from aged mice (Extended Data Fig. 8e,f), suggesting that mitophagy activity is required for spermidine effects on oocytes from aged mice.

Improvement of spermidine-induced oocyte quality is conserved across species

We next used porcine oocytes as a model to test the potential effects of spermidine on oocyte maturation in another species. As shown in Extended Data Fig. 9a,b, in vitro maturation of porcine oocytes as assessed by PB1 extrusion was substantially lower in the H_2O_2-treated group than in the controls, and maturation was restored after spermidine supplementation (Extended Data Fig. 9a,b). Furthermore, we found that spermidine supplementation recovered LC3 levels and mitochondrial dynamics in H_2O_2-treated porcine oocytes (Extended Data Fig. 9c–f), thus removing excessive ROS and inhibiting apoptosis (Extended Data Fig. 9g–j). Therefore, we demonstrate that the mechanism of action of spermidine on oocyte development under oxidative stress is highly conserved.

Discussion

Ovarian development in mammals is an orderly, coordinated, complicated and finely regulated physiological process that has been affected by multiple intrinsic and extrinsic factors to produce high-quality oocytes and thus guarantee female reproduction[25]. Among various contributors, metabolic regulation is one of the most pivotal factors. It has been widely reported that metabolic disorders can result in ovarian dysfunctions and affect female fertility[26]. For instance, polycystic ovarian syndrome is a common metabolic disorder in reproductive-age persons[27]. In addition, reproductive aging may impact female fertility by impairing metabolic homeostasis[28]. However, our current understanding regarding how metabolic changes influence the deterioration of germ cells during reproductive aging remains largely elusive.

To this end, we carried out untargeted metabolomics to compare metabolic profiles in ovaries between young and aged mice. Our metabolomic data identified that spermidine was remarkably reduced in ovaries from aged mice. Spermidine has been found to function as an autophagy inducer to participate in a diversity of cellular processes that are associated with the progression of aging across species[29]. Therefore, we proposed that spermidine might be a key metabolite

in maintaining the female reproductive lifespan. Interestingly, we also noticed that levels of several steroids such as pregnenolone, progesterone and hydroxyprogesterone were dramatically upregulated in ovaries of aged mice. However, a previous study has shown that plasma concentrations of these three steroids as measured by LC–MS/MS decline with advanced age in humans[30]. Whether this discrepancy is attributed to different tissue sources or species requires further investigation. In addition, there is conflicting evidence regarding the effects of progesterone levels on oocyte quality. It has been reported that the number of oocytes obtained during intracytoplasmic sperm-injection procedures is positively correlated with serum progesterone levels but negatively associated with follicular fluid progesterone levels[31]. Moreover, high levels of progesterone in human follicular fluid are positively correlated with oocyte quality as defined by subsequent embryonic development, implantation and pregnancy[32,33] but paradoxically are associated with polyspermy and multipronuclear embryos[34,35]. It appears that both reduced and excessive progesterone levels are detrimental to oocyte quality.

Female aging has been reported to compromise both nuclear and cytoplasmic maturation of oocytes including polar body extrusion, chromosome euploidy, CG dynamics, mitochondrial function, fertilization capacity and early embryonic development potential[36], although the degrees of influence fluctuate in different studies[37,38]. As our data presented similar defects induced by aging in mouse oocytes, we then supplemented aged mice with exogenous spermidine to assess its potential effects on the oocyte quality, ovarian function and female fertility. Our findings validated that in vivo supplementation with spermidine promoted oocyte maturation, fertilization and embryonic development, thereby increasing the fertility of aged mice. In addition, spermidine supplementation in the culture medium also enhanced the quality of oocytes from aged mice during in vitro maturation, documenting that spermidine can rejuvenate oocyte quality both in vivo and in vitro. It is worth noting that excessive spermidine is not necessarily beneficial to female reproduction as shown by our data that supplementation with 100 mg per kg spermidine resulted in a slower oocyte-maturation rate than that with 50 mg per kg spermidine. This is consistent with a previous study that found that supplementation with spermidine at supraphysiological doses in young female mice causes ovarian oxidative stress and induces granulosa cell apoptosis[39]. A similar phenomenon was observed in our recent study in that supplementation with NMN at higher doses did not obtain an optimal outcome for oocyte-maturation competency in aged mice[9]. As for the comparison between spermidine and NMN with regard to female reproductive improvements, it could not be made based on the current data, as we used mouse models at different ages in these two studies. The comparison or combination effects of spermidine and NMN with regard to oocyte quality and animal fertility need to be clarified in future work.

To gain insights into the mechanisms underlying spermidine's effect on oocytes from aged mice, we performed microtranscriptomic analysis to characterize potential downstream effectors. In agreement with previous studies that spermidine induces autophagy to protect against age-related pathologies[18,40], our RNA-seq data indicated that autophagy, mitophagy and mitochondrial function were the main pathways by which spermidine restored oocyte quality in aged mice. Subsequent investigations verified that spermidine elevated autophagy to restore mitophagy activity and mitochondrial function in oocytes from aged mice, hence inhibiting excessive ROS production and apoptosis induced by aging. As one of the important hallmarks of oocyte aging is the generation of oxidative stress, we then used H_2O_2 treatment to partially mimic the phenotypes induced by aging in porcine oocytes, including oocyte meiotic failure, mitochondrial dysfunction, impaired autophagy and apoptosis, certifying that the beneficial effects of spermidine on oocyte maturation were conserved across species. Intriguingly, spermidine has been identified as an important mating component to promote fertilization

in an autophagy-independent manner in *Saccharomyces cerevisiae* and *Caenorhabditis elegans*[41], suggesting that spermidine might regulate reproductive processes through multiple mechanisms.

In sum, based on ovarian metabolomic data and much in vivo and in vitro experimental evidence, we demonstrate that spermidine is a critical metabolite for preserving oocyte quality during aging. Supplementation with spermidine can promote oocyte maturation, enhance fertilization capacity as well as early embryonic development potential and thus increase female fertility in aged animals. Notably, spermidine strengthens mitophagy activity to maintain mitochondrial function and to suppress apoptosis in oocytes from aged mice (Supplementary Fig. 1). Thus, our study provides clinical implications for the potential application of spermidine to ameliorate the reproductive outcome of women at an advanced age by means of either natural pregnancy or assisted reproductive technology.

Methods

Mice and spermidine supplementation

All animal protocols and experimental procedures were approved by the Animal Research Institute Committee of Nanjing Agricultural University, China. Young (~6–8-week-old) and aged (~52–56-week-old) ICR female mice were housed with a 12-h light–dark cycle, constant temperature and free access to food and water. Aged mice were intraperitoneally injected daily with spermidine (Sigma-Aldrich; 50 mg per kg body weight per d, dissolved in PBS) or the equivalent volume of PBS according to previous studies[42,43] for 10 consecutive days. Alternatively, aged mice were supplemented with spermidine at 3 mM in drinking water as previously reported for 30 d[44,45].

Metabolomic analysis

The non-targeted metabolomic analysis was performed at the Beijing Genomics Institute (Shenzhen, China) on a platform consisting of an independent ultra-high-performance liquid chromatography–tandem mass spectrometry (UPLC–MS/MS) instrument. Briefly, five replicates of samples for each group (50 mg ovarian tissue per replicate) were collected for metabolite extraction. The supernatants were then analyzed using a Waters UPLC I-Class PLUS (Waters) tandem Q Exactive high-resolution mass spectrometer (Thermo Fisher Scientific) for separation and detection of metabolites. After importing the offline mass spectrometry data into Compound Discoverer 3.3 software (Thermo Fisher Scientific) and combined analysis with the ChemSpider online database, the mzCloud database and the bmdb database (Beijing Genomics Institute metabolome database), data information including metabolite peak area and identification results was obtained. MetaX was then used for data processing of the result file from Compound Discoverer to screen for differential metabolites and enriched metabolic pathways.

Antibodies and dyes

Mouse monoclonal anti-α-tubulin–fluorescein isothiocyanate (FITC) antibody and LCA–FITC were purchased from Sigma-Aldrich. Rabbit monoclonal anti-γH2AX antibody and rabbit polyclonal anti-microtubule-associated protein 1 LC3B antibody were purchased from Cell Signaling Technology. The human anti-centromere antibody was obtained from Antibodies. The mouse monoclonal anti-ASTL antibody was purchased from Santa Cruz Biotechnology. The rabbit monoclonal anti-VDAC1 antibody was purchased from ABclonal Technology.

Measurement of spermidine levels

The level of spermidine was quantified with an enzyme-linked immunosorbent assay kit (Cloud-Clone) according to the manufacturer's instructions. In brief, supernatants collected from mouse ovarian lysates were centrifuged at 10,000g for 20 min. Next, 50 µl of supernatant and an equal volume of Detection Reagent A were added to each well of a plate followed by incubation for 1 h at 37 °C. Detection Reagent

B (100 µl) was added to the wells after three washes, and samples were incubated for 30 min at 37 °C. After another five washes, 90 µl substrate solution was added to each well, and samples were incubated for 10 min at 37 °C, followed by the addition of 50 µl stop solution. Finally, the plate was mixed and immediately measured at 450 nm with a spectrophotometer (Thermo Fisher Scientific). Analysis was carried out by back calculation to the standard curve.

Oocyte collection and maturation

Female mice were intraperitoneally injected with 10 IU PMSG and humanely euthanized after 48 h to collect oocytes at the GV stage. GV oocytes were cultured in M16 medium for 14 h at 37 °C with 5% CO_2 for in vitro maturation. For collection of ovulated oocytes, female mice were injected with 10 IU PMSG followed by 10 IU hCG 48 h later. Oocytes were collected from oviductal ampullae at -13–14 h after hCG injection and briefly exposed to 1 mg ml^{-1} hyaluronidase to remove cumulus cells.

Histological analysis and follicle quantification

Ovaries were fixed in 4% paraformaldehyde, dehydrated and embedded in paraffin and then sectioned at a thickness of 8 µm for hematoxylin and eosin staining.

Quantification of ovarian follicles was carried out as previously described[46,47]. Briefly, follicles were scored in every fifth section (40-µm interval), and, in each section, only those follicles with a clear oocyte nucleus were counted and multiplied by 5 to calculate the total number of follicles in an ovary. Ovarian follicles at different developmental stages were distinguished from each other as follows according to the well-accepted standards established by Peterson and Peters[48]: primordial follicles (types 1 and 2, small oocytes without attached cells or surrounded by several flattened pre-granulosa cells), primary follicles (type 3, middle-sized oocytes surrounded by a single layer of cubical granulosa cells), secondary follicles (types 4 and 5, large oocytes surrounded by more than two layers of granulosa cells), pre-antral follicles (type 6, large oocytes surrounded by many layers of granulosa cells with several small cavities) and antral follicles (types 7 and 8, follicles with a single big cavity).

TUNEL staining was carried out using the FITC TUNEL Cell Apoptosis Detection Kit according to the manufacturer's instructions (Servicebio).

Fluorescence staining and measurement

Antibody staining, mitochondrion staining, JC-1 staining, DCFH staining, annexin V staining and fluorescence intensity measurements were performed using the protocols described in our previous study[9]. The primary antibodies and dyes used are listed as follows: anti-α-tubulin–FITC antibody (1:200), anti-centromere antibody (1:200), anti-ovastacin antibody (1:100), anti-γH2AX antibody (1:100), anti-LCA–FITC (1:100), anti-LC3B antibody (1:100) and anti-VDAC1 antibody (1:100).

For lysosome staining, oocytes were incubated in M16 medium containing 100 nM cell-permeant LysoTracker Green (Beyotime Biotech) at 37 °C in a dark environment with 5% CO_2 in air for 30 min. After three washes with fresh M2 medium, samples were mounted on glass slides and imaged with the LSM 900 confocal microscope system (Carl Zeiss).

Colocalization was measured with PCC and MCC using Coloc2 in Fiji as reported previously[49,50]. PCC values ranged from 1 for positive correlation of two images to −1 for negative correlation of two images. Among MCC coefficients, MCC-M1 and MCC-M2 were used to denote the proportion of each protein that colocalized with the other. MCC values ranged from 0 for no colocalization to 1 for complete colocalization.

Chromosome spreading and kinetochore staining

ZP were removed from oocytes by exposure to Tyrode's buffer (pH 2.5) at 37 °C for ~30 s. ZP-free oocytes were then fixed in a solution

containing 1% paraformaldehyde and 0.15% Triton X-100 on a glass slide and air dried, followed by incubation with anti-centromere antibody (1:200) at 4 °C overnight and Alexa Fluor 555-conjugated secondary antibody for 1 h for kinetochore staining. Chromosomes were then counterstained with Hoechst 33342 and imaged by confocal microscopy.

Sperm-binding assay
The sperm-binding assay was performed as we described previously[9].

In vivo fertilization and in vitro embryo culture
To collect embryos, female mice were mated overnight with male mice of proven fertility following sequential injections with 10 IU PMSG and 10 IU hCG. Zygotes were obtained by flushing the ampulla of oviducts ~13–14 h after hCG injection and cultured in vitro in KSOM medium (Aibei Biotech) at 37 °C in an atmosphere with 5% CO_2 for 24 h to yield two-cell embryos and for 84 h to yield blastocysts.

Microtranscriptome sequencing and RNA library construction
Microtranscriptomic analysis of GV oocytes was carried out using a protocol for SMART-seq2. In brief, three or four sets of samples were collected for each group (ten oocytes per sample) in lysis buffer. The procedures for library preparation were conducted as we described previously[9].

RNA isolation and quantitative real-time PCR
A total of 30 oocytes were collected for RNA extraction using the Dynabeads mRNA DIRECT Kit (Thermo Fisher Scientific), followed by cDNA synthesis using HiScript II RT SuperMix (Vazyme). RT–qPCR was performed using ChamQ SYBR qPCR Master Mix (Vazyme) and the QuantStudio 7 Flex Real-Time PCR System (Thermo Fisher Scientific). Relative mRNA levels were normalized against values from *Gadph* mRNA, and quantification of fold change was determined by the comparative Ct method. Primers were synthesized by Sangon Biotech, and their sequences are listed in Supplementary Table 1.

Porcine oocyte collection and in vitro maturation
The procedures for porcine oocyte collection and in vitro maturation were performed as we described previously[51].

Statistics and reproducibility
No statistical methods were used to predetermine sample sizes, but our sample sizes are similar to those reported in previous publications[9,52,53]. Data collection and analysis were not performed blinded to the conditions of the experiments, and no data were excluded from the analyses. All statistical data from at least three independent experiments are presented as mean ± s.e.m. or s.d. unless otherwise stated, and the number of samples used in each group is labeled in parentheses as (*n*). Data were analyzed by two-tailed unpaired *t*-test following the Shapiro–Wilk test for normality, which is provided by GraphPad Prism 8 statistical software. $P < 0.05$ was considered statistically significant.

Reporting summary
Further information on research design is available in the Nature Portfolio Reporting Summary linked to this article.

Data availability
Transcriptomic raw data have been deposited in the Gene Expression Omnibus database under accession number GSE239551.

References

1. Wasielak-Politowska, M. & Kordowitzki, P. Chromosome segregation in the oocyte: what goes wrong during aging. *Int. J. Mol. Sci.* **23**, 2880 (2022).
2. Kim, H. O., Sung, N. & Song, I. O. Predictors of live birth and pregnancy success after in vitro fertilization in infertile women aged 40 and over. *Clin. Exp. Reprod. Med.* **44**, 111–117 (2017).
3. du Fosse, N. A., van der Hoorn, M. P., van Lith, J. M. M., le Cessie, S. & Lashley, E. Advanced paternal age is associated with an increased risk of spontaneous miscarriage: a systematic review and meta-analysis. *Hum. Reprod. Update* **26**, 650–669 (2020).
4. Seshadri, S., Morris, G., Serhal, P. & Saab, W. Assisted conception in women of advanced maternal age. *Best Pract. Res. Clin. Obstet. Gynaecol.* **70**, 10–20 (2021).
5. Raz, N. et al. Cumulative pregnancy and live birth rates through assisted reproduction in women 44–45 years of age: is there any hope? *J. Assist. Reprod. Genet.* **35**, 441–447 (2018).
6. Humm, K. C. et al. In vitro fertilization in women under 35: counseling should differ by age. *J. Assist. Reprod. Genet.* **32**, 1449–1457 (2015).
7. Mikwar, M., MacFarlane, A. J. & Marchetti, F. Mechanisms of oocyte aneuploidy associated with advanced maternal age. *Mutat. Res. Rev. Mutat. Res.* **785**, 108320 (2020).
8. Miao, Y., Chen, J., Gao, Q. & Xiong, B. Generation and assessment of high-quality mouse oocytes and embryos following nicotinamide mononucleotide administration. *STAR Protoc.* **2**, 100298 (2021).
9. Miao, Y., Cui, Z., Gao, Q., Rui, R. & Xiong, B. Nicotinamide mononucleotide supplementation reverses the declining quality of maternally aged oocytes. *Cell Rep.* **32**, 107987 (2020).
10. Bertoldo, M. J. et al. NAD⁺ repletion rescues female fertility during reproductive aging. *Cell Rep.* **30**, 1670–1681 (2020).
11. Kramer, D. L. et al. Polyamine acetylation modulates polyamine metabolic flux, a prelude to broader metabolic consequences. *J. Biol. Chem.* **283**, 4241–4251 (2008).
12. Soda, K. Overview of polyamines as nutrients for human healthy long life and effect of increased polyamine intake on DNA methylation. *Cells* **11**, 164 (2022).
13. Ni, Y. Q. & Liu, Y. S. New insights into the roles and mechanisms of spermidine in aging and age-related diseases. *Aging Dis.* **12**, 1948–1963 (2021).
14. Bae, D. H., Lane, D. J. R., Jansson, P. J. & Richardson, D. R. The old and new biochemistry of polyamines. *Biochim. Biophys. Acta Gen. Subj.* **1862**, 2053–2068 (2018).
15. Fan, J., Feng, Z. & Chen, N. Spermidine as a target for cancer therapy. *Pharmacol. Res.* **159**, 104943 (2020).
16. Lefevre, P. L., Palin, M. F. & Murphy, B. D. Polyamines on the reproductive landscape. *Endocr. Rev.* **32**, 694–712 (2011).
17. Partridge, L., Fuentealba, M. & Kennedy, B. K. The quest to slow ageing through drug discovery. *Nat. Rev. Drug Discov.* **19**, 513–532 (2020).
18. Eisenberg, T. et al. Induction of autophagy by spermidine promotes longevity. *Nat. Cell Biol.* **11**, 1305–1314 (2009).
19. Morselli, E. et al. Spermidine and resveratrol induce autophagy by distinct pathways converging on the acetylproteome. *J. Cell Biol.* **192**, 615–629 (2011).
20. Gupta, V. K. et al. Restoring polyamines protects from age-induced memory impairment in an autophagy-dependent manner. *Nat. Neurosci.* **16**, 1453–1460 (2013).
21. Wang, I. F. et al. Autophagy activators rescue and alleviate pathogenesis of a mouse model with proteinopathies of the TAR DNA-binding protein 43. *Proc. Natl Acad. Sci. USA* **109**, 15024–15029 (2012).
22. Eisenberg, T. et al. Cardioprotection and lifespan extension by the natural polyamine spermidine. *Nat. Med.* **22**, 1428–1438 (2016).
23. Zhang, M., Lu, Y., Chen, Y., Zhang, Y. & Xiong, B. Insufficiency of melatonin in follicular fluid is a reversible cause for advanced maternal age-related aneuploidy in oocytes. *Redox Biol.* **28**, 101327 (2020).
24. Ben-Meir, A. et al. Coenzyme Q10 restores oocyte mitochondrial function and fertility during reproductive aging. *Aging Cell* **14**, 887–895 (2015).

25. Grive, K. J. & Freiman, R. N. The developmental origins of the mammalian ovarian reserve. *Development* **142**, 2554–2563 (2015).
26. Dri, M., Klinger, F. G. & De Felici, M. The ovarian reserve as target of insulin/IGF and ROS in metabolic disorder-dependent ovarian dysfunctions. *Reprod. Fertil.* **2**, R103–R112 (2021).
27. Randeva, H. S. et al. Cardiometabolic aspects of the polycystic ovary syndrome. *Endocr. Rev.* **33**, 812–841 (2012).
28. Della Torre, S., Benedusi, V., Fontana, R. & Maggi, A. Energy metabolism and fertility: a balance preserved for female health. *Nat. Rev. Endocrinol.* **10**, 13–23 (2014).
29. Madeo, F., Bauer, M. A., Carmona-Gutierrez, D. & Kroemer, G. Spermidine: a physiological autophagy inducer acting as an anti-aging vitamin in humans? *Autophagy* **15**, 165–168 (2019).
30. Eisenhofer, G. et al. Reference intervals for plasma concentrations of adrenal steroids measured by LC–MS/MS: impact of gender, age, oral contraceptives, body mass index and blood pressure status. *Clin. Chim. Acta* **470**, 115–124 (2017).
31. Pizarro, B. M. et al. Estradiol and progesterone levels are related to redox status in the follicular fluid during in vitro fertilization. *J. Endocr. Soc.* **4**, bvaa064 (2020).
32. O'Brien, Y., Wingfield, M. & O'Shea, L. C. Anti-mullerian hormone and progesterone levels in human follicular fluid are predictors of embryonic development. *Reprod. Biol. Endocrinol.* **17**, 47 (2019).
33. Revelli, A. et al. Follicular fluid content and oocyte quality: from single biochemical markers to metabolomics. *Reprod. Biol. Endocrinol.* **7**, 40 (2009).
34. Hillier, S. G., Wickings, E. J., Afnan, M., Margara, R. A. & Winston, R. M. Granulosa cell steroidogenesis before in vitro fertilization. *Biol. Reprod.* **31**, 679–686 (1984).
35. Ben-Rafael, Z. et al. Relationships between polypronuclear fertilization and follicular fluid hormones in gonadotropin-treated women. *Fertil. Steril.* **47**, 284–288 (1987).
36. Miao, Y. L., Kikuchi, K., Sun, Q. Y. & Schatten, H. Oocyte aging: cellular and molecular changes, developmental potential and reversal possibility. *Hum. Reprod. Update* **15**, 573–585 (2009).
37. Liu, C. et al. Granulosa cell mevalonate pathway abnormalities contribute to oocyte meiotic defects and aneuploidy. *Nat. Aging* **3**, 670–687 (2023).
38. Selesniemi, K., Lee, H. J., Muhlhauser, A. & Tilly, J. L. Prevention of maternal aging-associated oocyte aneuploidy and meiotic spindle defects in mice by dietary and genetic strategies. *Proc. Natl Acad. Sci. USA* **108**, 12319–12324 (2011).
39. Jiang, D. et al. Spermidine at supraphysiological doses induces oxidative stress and granulosa cell apoptosis in mouse ovaries. *Theriogenology* **168**, 25–32 (2021).
40. Hofer, S. J. et al. Spermidine-induced hypusination preserves mitochondrial and cognitive function during aging. *Autophagy* **17**, 2037–2039 (2021).
41. Bauer, M. A. et al. Spermidine promotes mating and fertilization efficiency in model organisms. *Cell Cycle* **12**, 346–352 (2013).
42. Yang, Q. et al. Spermidine alleviates experimental autoimmune encephalomyelitis through inducing inhibitory macrophages. *Cell Death Differ.* **23**, 1850–1861 (2016).
43. Baek, A. R. et al. Spermidine attenuates bleomycin-induced lung fibrosis by inducing autophagy and inhibiting endoplasmic reticulum stress (ERS)-induced cell death in mice. *Exp. Mol. Med.* **52**, 2034–2045 (2020).
44. Zhou, J. et al. Spermidine-mediated hypusination of translation factor EIF5A improves mitochondrial fatty acid oxidation and prevents non-alcoholic steatohepatitis progression. *Nat. Commun.* **13**, 5202 (2022).
45. Liu, S. et al. Effects of spermidine on gut microbiota modulation in experimental abdominal aortic aneurysm mice. *Nutrients* **14**, 3349 (2022).
46. Liu, L. et al. Infertility caused by retardation of follicular development in mice with oocyte-specific expression of Foxo3a. *Development* **134**, 199–209 (2007).
47. Jiang, Z. Z. et al. LKB1 acts as a critical gatekeeper of ovarian primordial follicle pool. *Oncotarget* **7**, 5738–5753 (2016).
48. Pedersen, T. & Peters, H. Proposal for a classification of oocytes and follicles in the mouse ovary. *J. Reprod. Fertil.* **17**, 555–557 (1968).
49. Fan, X. Y. et al. Reduction of mtDNA heteroplasmy in mitochondrial replacement therapy by inducing forced mitophagy. *Nat. Biomed. Eng.* **6**, 339–350 (2022).
50. Losinno, A. D., Martinez, S. J., Labriola, C. A., Carrillo, C. & Romano, P. S. Induction of autophagy increases the proteolytic activity of reservosomes during *Trypanosoma cruzi* metacyclogenesis. *Autophagy* **17**, 439–456 (2021).
51. Miao, Y., Cui, Z., Zhu, X., Gao, Q. & Xiong, B. Supplementation of nicotinamide mononucleotide improves the quality of postovulatory aged porcine oocytes. *J. Mol. Cell Biol.* **14**, mjac025 (2022).
52. Zhou, C. et al. The cohesin stabilizer sororin drives G_2–M transition and spindle assembly in mammalian oocytes. *Sci. Adv.* **7**, eabg9335 (2021).
53. Zhou, C. et al. The cohesin release factor Wapl interacts with Bub3 to govern SAC activity in female meiosis I. *Sci. Adv.* **6**, eaax3969 (2020).

Author contributions

B.X. designed the research; Y.Z., J.B., Z.C., Y.L., Q.G. and Y.M. performed experiments; Y.Z. and B.X. analyzed data; Y.Z. and B.X. wrote the manuscript.

Competing interests

The authors declare no competing interests.

Additional information

Supplementary information The online version contains supplementary material available at https://doi.org/10.1038/s43587-023-00498-8.

Correspondence and requests for materials should be addressed to Bo Xiong.
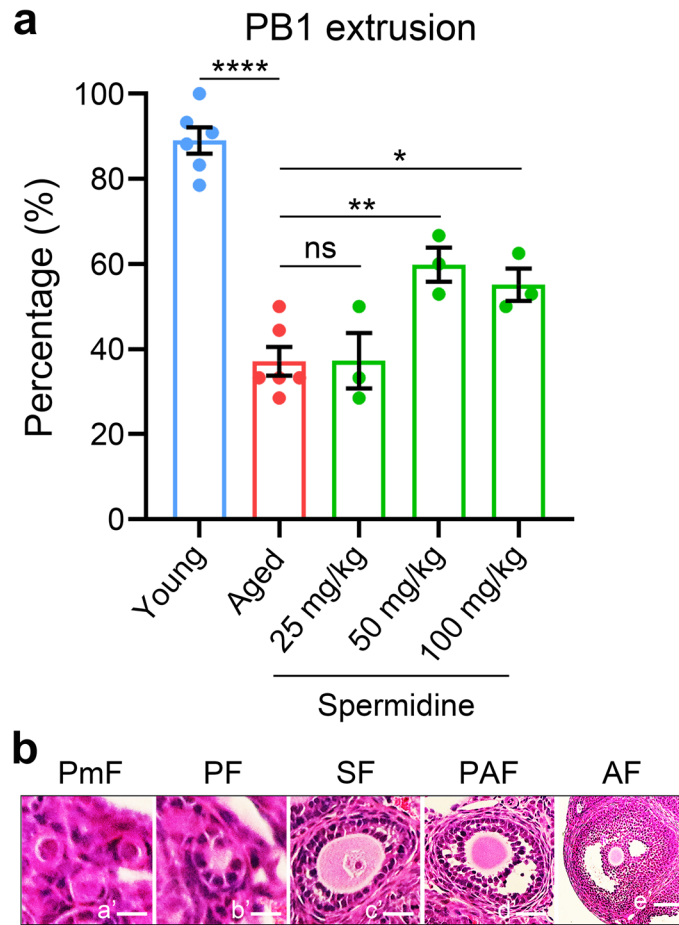
Peer review information *Nature Aging* thanks Elnur Babayev, Heng-Yu, and the other, anonymous, reviewer(s) for their contribution to the peer review of this work.

Reprints and permissions information is available at www.nature.com/reprints.

a

b

Extended Data Fig. 1 | Supplementary data related to Fig. 2. a, Effects of different doses of spermidine on the *in vivo* maturation of aged oocytes. The percentage of PB1 extrusion was quantified in young (n = 132), aged (n = 71), and SPD+aged (25 mg/kg: n = 30, 50 mg/kg: n = 36, 100 mg/kg: n = 31) oocytes. ****P < 0.0001, P = 0.9842, **P = 0.0046, *P = 0.0135. ns, no significance. Data were expressed as mean percentage (mean ± SEM) of at least three independent experiments. Statistical significance was determined by two-tailed unpaired *t*-test. **b**, Representative images of follicles at different developmental stages in young mice. PmF, primordial follicle, small oocytes without attached cells or surrounded by several flattened pre-granulosa cells; PF, primary follicle, middle sized oocytes surrounded by a single layer of cubical granulosa cells; SF, secondary follicle, large oocytes surrounded by more than two layers of granulosa cells; PAF, pre-antral follicle, large oocytes surrounded by many layers of granulosa cells with several small cavities; AF, antral follicle, follicles with a single big cavity. Scale bars: a', 10 μm; b', 20 μm; c', 25 μm; d', 60 μm; e', 150 μm.
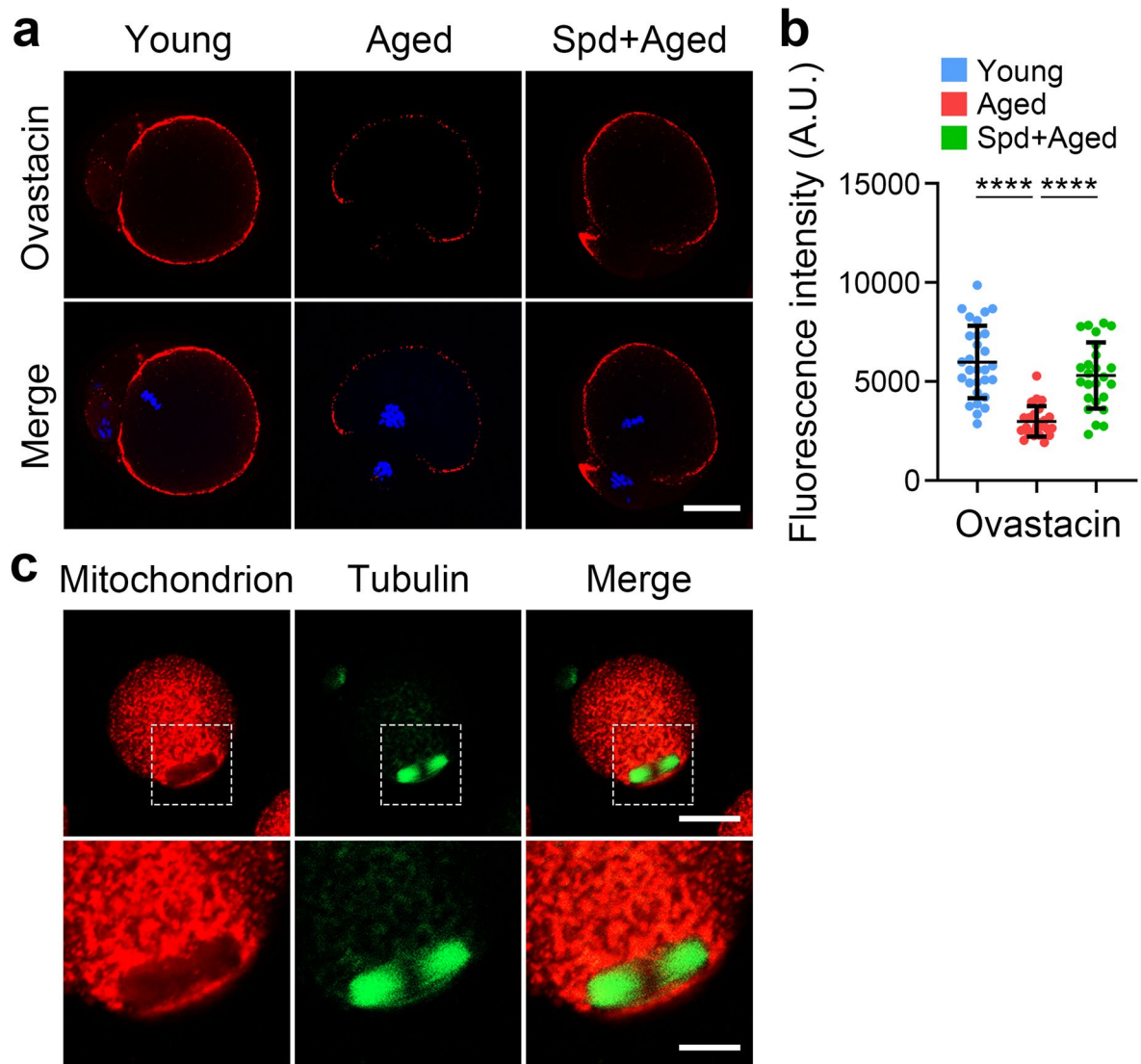
Extended Data Fig. 2 | Supplementary data related to Fig. 4. a, Representative images of ovastacin in young, aged, and Spd+aged M II oocytes. Scale bar, 30 μm. **b,** The fluorescence intensity of ovastacin signals was measured in young (n = 29), aged (n = 25), and Spd+aged (n = 25) M II oocytes. ****P < 0.0001, ****P < 0.0001. Data were expressed as mean value (mean ± SD) of at least three independent experiments. Statistical significance was determined by two-tailed unpaired *t*-test. **c,** Co-staining of mitochondrion and spindle in young M II oocytes. Scale bars, 40 μm, 20 μm.
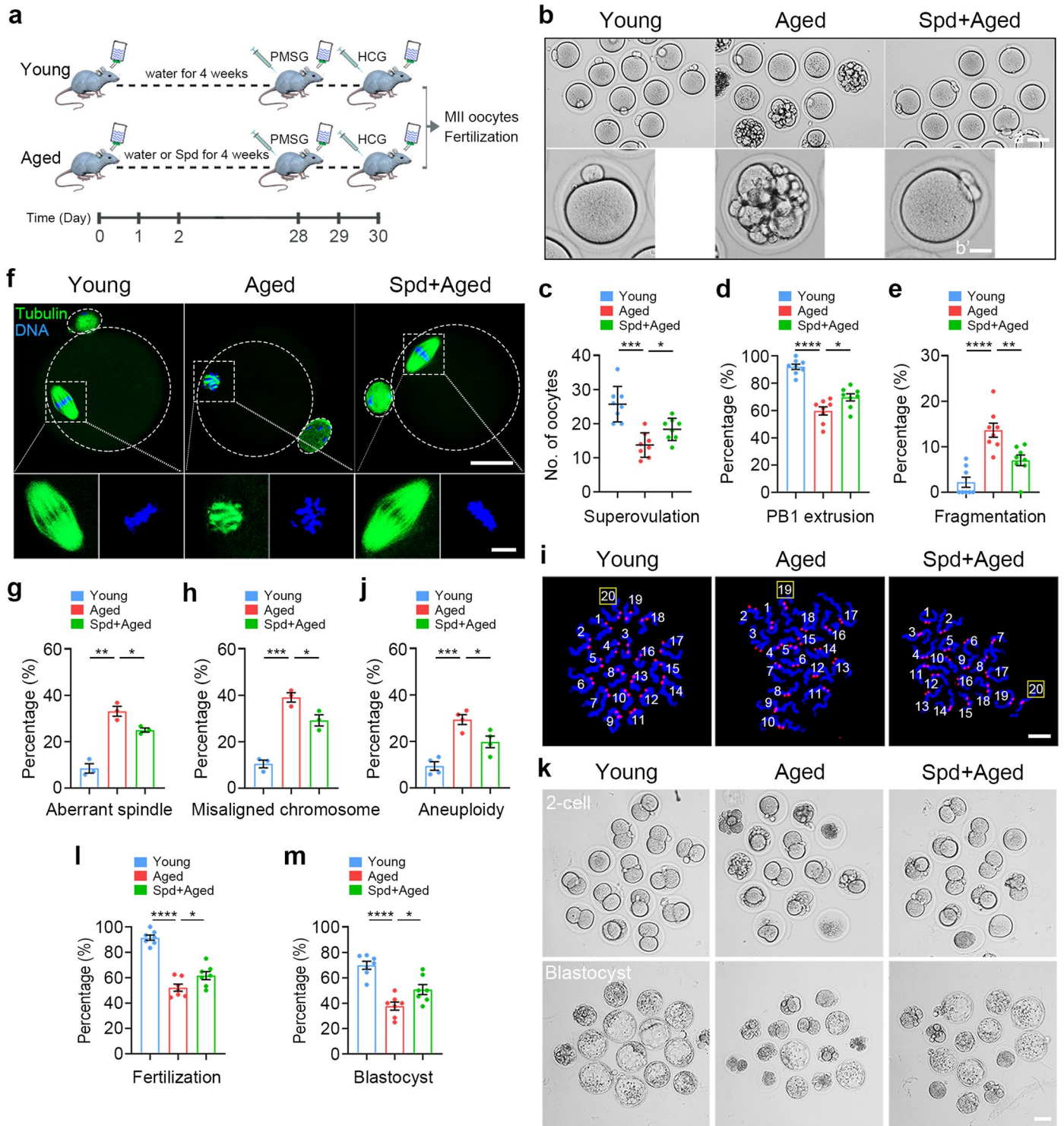
Extended Data Fig. 3 | See next page for caption.

Extended Data Fig. 3 | Effects of dietary supplementation of spermidine on the quality of aged oocytes. a, A timeline scheme for dietary spermidine supplementation, hormone priming and subsequent analyses. **b**, Representative images of *in vivo* matured oocytes collected from young, aged, and Spd+aged mice. Scale bars: a', 80 μm; b', 20 μm. **c**, The number of ovulated oocytes was counted in young (n = 8), aged (n = 8), and Spd+aged (n = 8) mice. ***P = 0.0001, *P = 0.0176. **d**, The percentage of PB1 extrusion was quantified in young (n = 206), aged (n = 110), and Spd+aged (n = 147) oocytes. ****P < 0.0001, *P = 0.0264. **e**, The proportion of fragmentation was quantified in young (n = 206), aged (n = 110), and Spd+aged (n = 147) oocytes. ****P < 0.0001, **P = 0.0042. **f**, Representative images of the spindle morphology and chromosome alignment in young, aged, and Spd+aged oocytes at M II stage. Scale bars, 30 μm, 10 μm. **g**, The percentage of aberrant spindles was quantified in young (n = 47), aged (n = 51), and Spd+aged (n = 48) M II oocytes. **P = 0.0011, *P = 0.0252. **h**, The percentage of misaligned chromosomes was quantified in young (n = 47), aged (n = 51), and Spd+aged (n = 48) M II oocytes. ***P = 0.0004, *P = 0.0345. **i**, Representative images of chromosome numbers in young, aged, and Spd+aged M II oocytes. Scale bar, 2.5 μm. **j**, The proportion of aneuploidy was quantified in young (n = 64), aged (n = 68), and Spd+aged (n = 65) M II oocytes. ***P = 0.0004, *P = 0.0265. **k**, Representative images of 2-cell embryos and blastocysts developed from *in vivo* fertilized young, aged, and Spd+aged oocytes. Scale bar, 50 μm. **l**, The fertilization rate was quantified in the young (n = 135), aged (n = 96), and Spd+aged (n = 94) groups. ****P < 0.0001, *P = 0.0442. **m**, The proportion of blastocyst formation was quantified in the young (n = 135), aged (n = 96), and Spd+aged (n = 94) groups. ****P < 0.0001, *P = 0.0254. Data in **c-e**, **g**, **h**, **j**, **l** and **m** were expressed as mean value (mean ± SD) or mean percentage (mean ± SEM) of at least three independent experiments. Statistical significance was determined by two-tailed unpaired *t*-test.
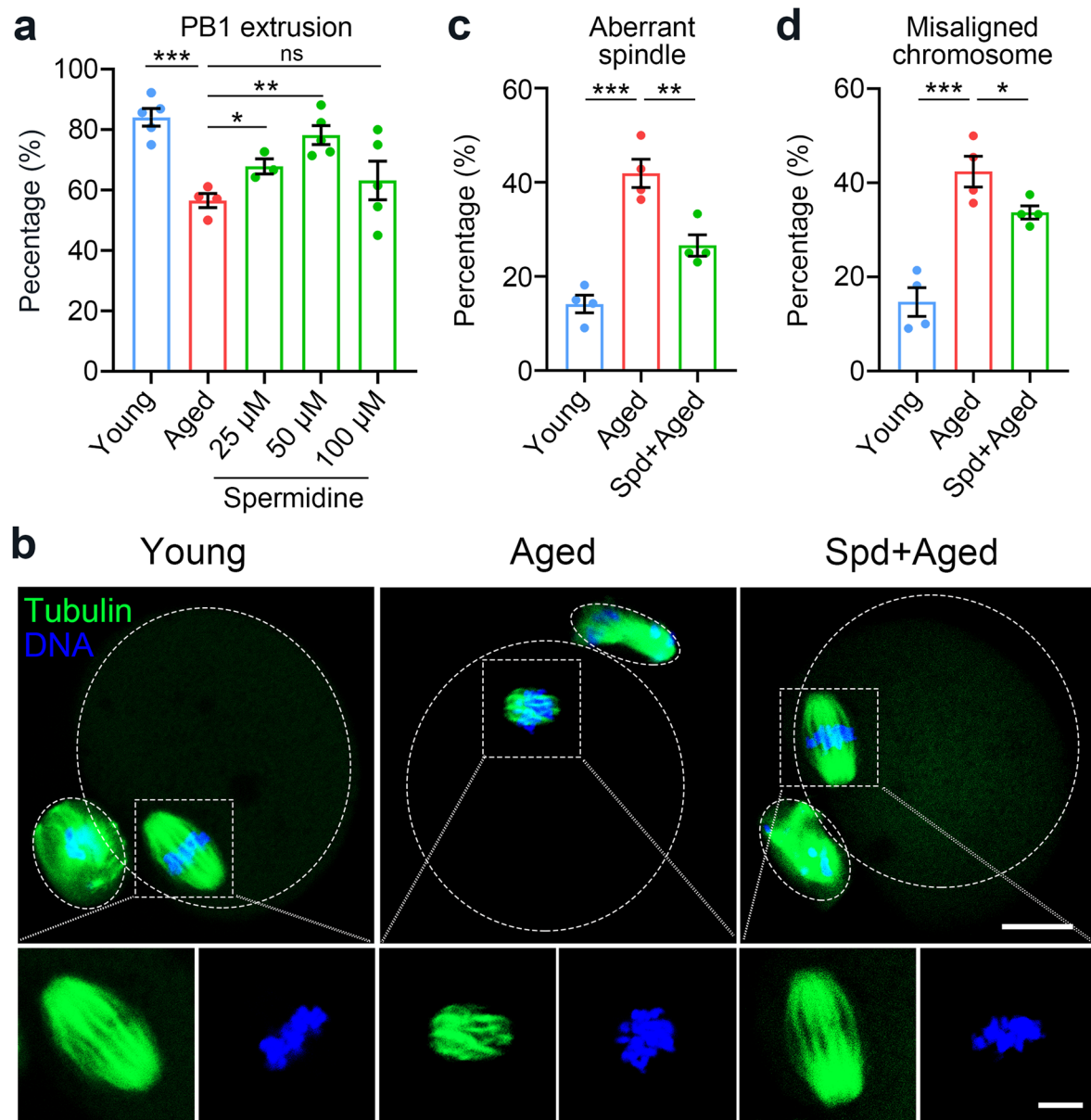
Extended Data Fig. 4 | Effects of spermidine supplementation on the in vitro maturation and spindle/chromosome structure in aged oocytes. a, The percentage of PB1 extrusion was quantified in young (n = 150), aged (n = 112), and Spd+aged (25 μM: n = 85, 50 μM: n = 136, 100 μM: n = 128) oocytes after *in vitro* maturation for 14 h. ***P = 0.0002, *P = 0.0223, **P = 0.0011, P = 0.4078. ns, no significance. **b**, Representative images of the spindle morphology and chromosome alignment in young, aged, and Spd+aged oocytes matured *in vitro*.

Scale bars, 20 μm, 5 μm. **c**, The percentage of aberrant spindles was quantified in young (n = 56), aged (n = 50), and Spd+aged (n = 56) oocytes matured *in vitro*. ***P = 0.0002, **P = 0.0067. **d**, The percentage of misaligned chromosomes was quantified in young (n = 56), aged (n = 50), and Spd+aged (n = 56) oocytes matured *in vitro*. ***P = 0.0008, *P = 0.0499. Data in **a**, **c** and **d** were expressed as mean percentage (mean ± SEM) of at least three independent experiments. Statistical significance was determined by two-tailed unpaired *t*-test.
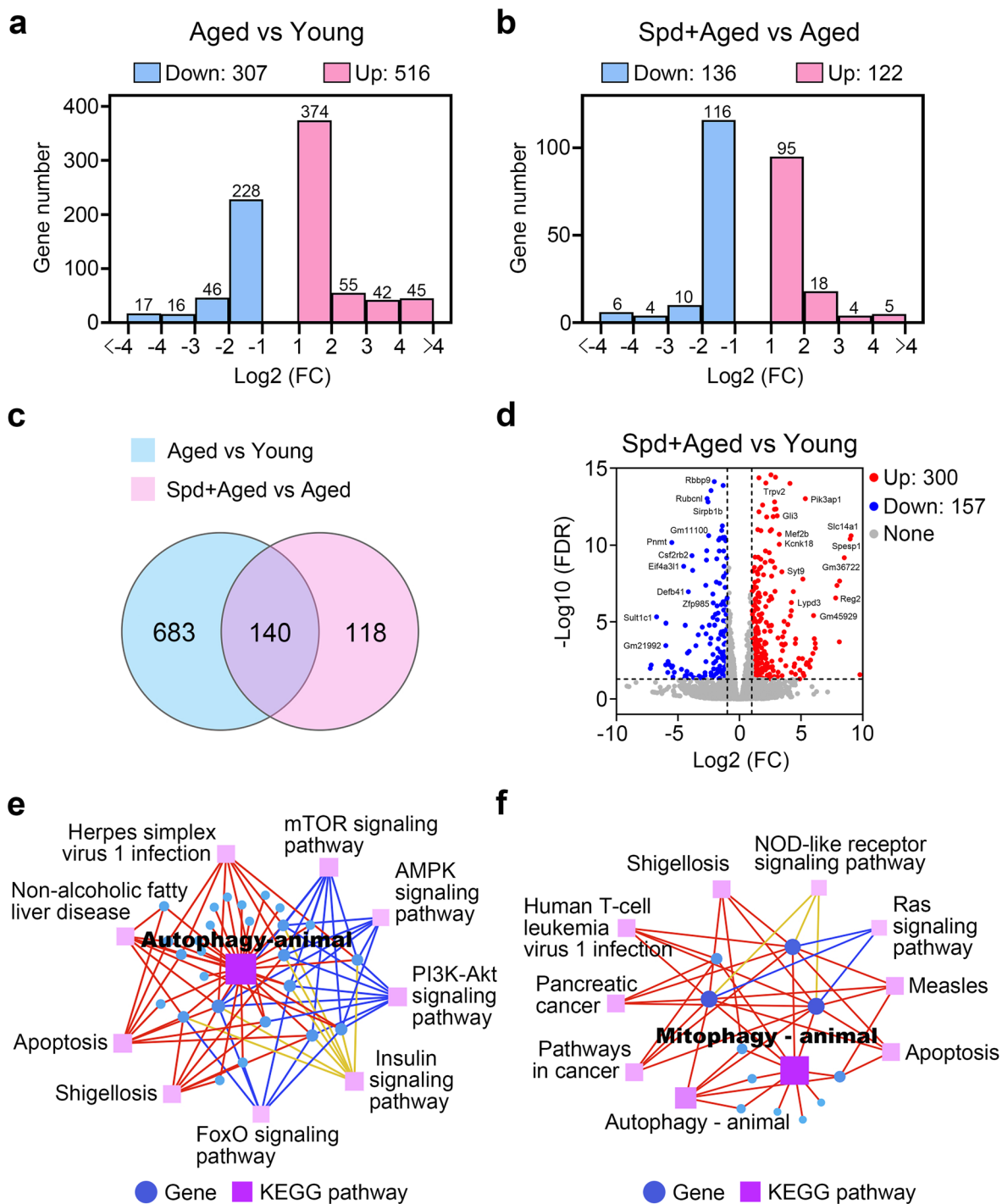
Extended Data Fig. 5 | Supplementary transcriptome data. a, The number of DEGs that were upregulated (red) and downregulated (blue) in aged oocytes compared to young controls. **b**, The number of DEGs that were upregulated (red) and downregulated (blue) in Spd+aged oocytes compared to aged ones. **c**, Venn diagram displayed the number of overlapping DEGs between aged compared to young group and Spd+aged compared to aged group. **d**, Volcano plot showed DEGs (upregulated, red; downregulated, blue) in Spd+aged oocytes compared to young ones. Some highly different DEGs were listed. **e**, KEGG interaction network of DEGs in the autophagy pathway. **f**, KEGG interaction network of DEGs in the mitophagy pathway.
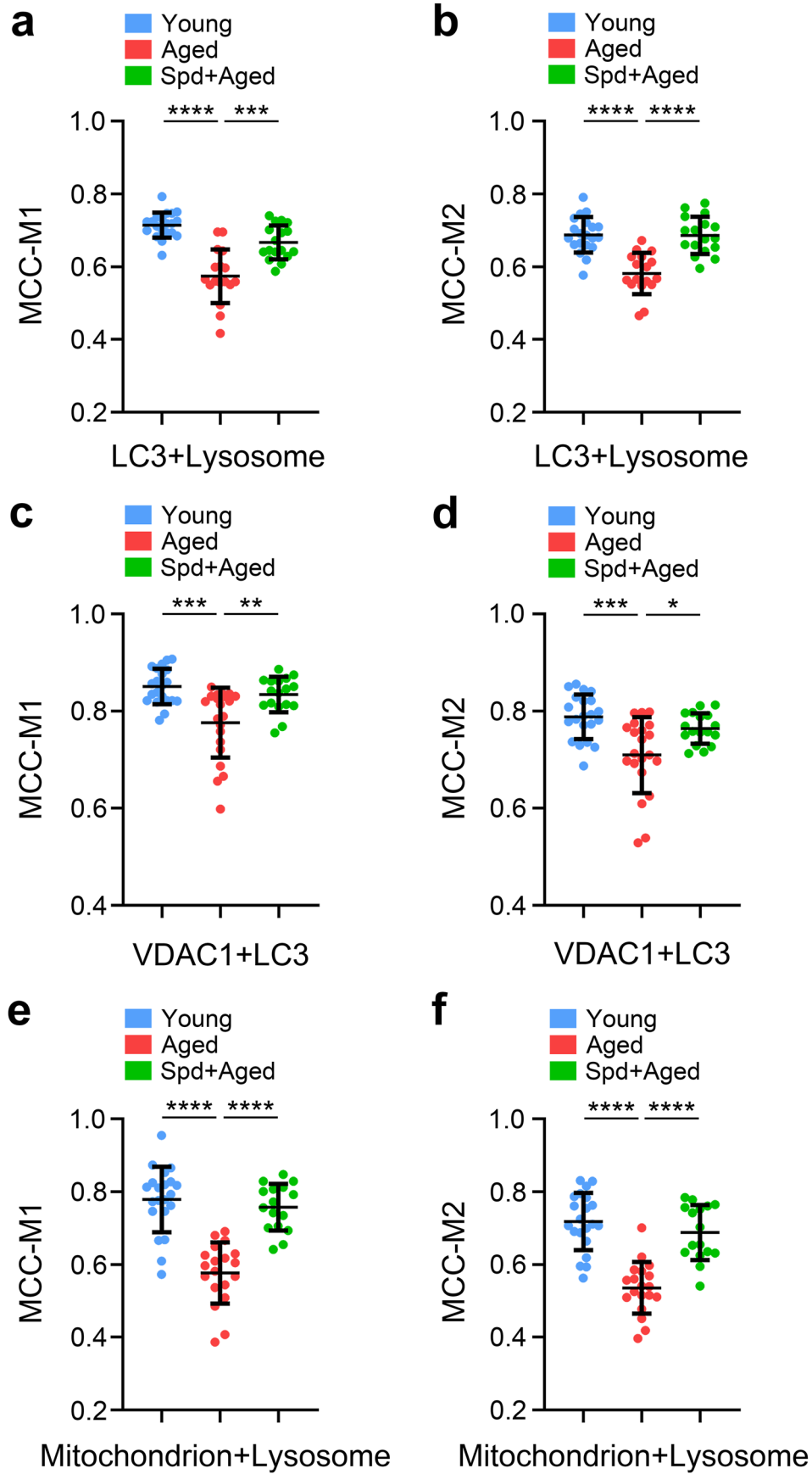
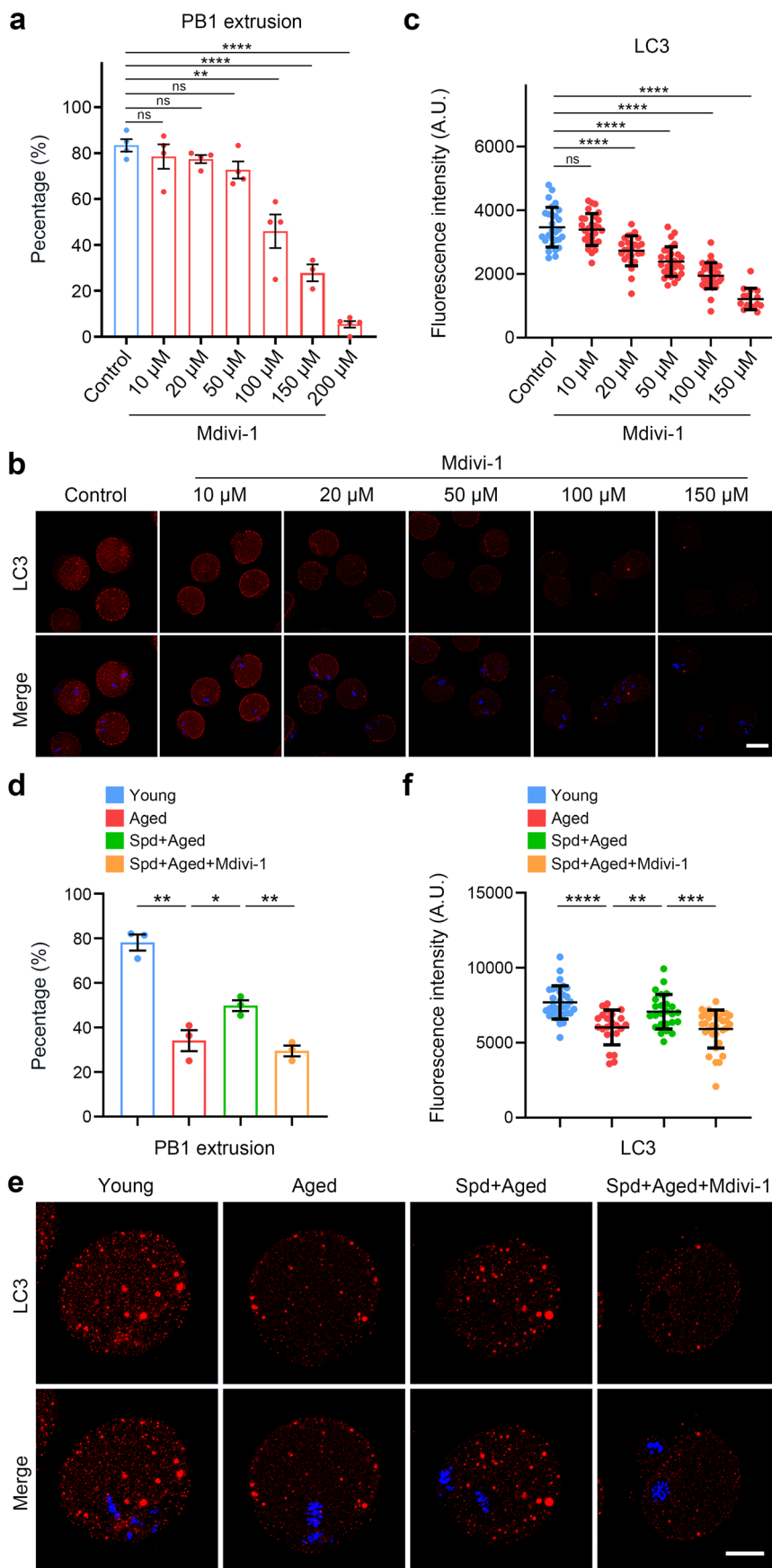**Extended Data Fig. 6 | See next page for caption.**

Extended Data Fig. 6 | Co-localization of two fluorescent signals as assessed by Mander's correlation coefficient. a, The MCC-M1 of LC3 and lysosome signals was calculated in young (n = 20), aged (n = 17), and Spd+aged (n = 17) M II oocytes. ****P < 0.0001, ***P = 0.0001. **b**, The MCC-M2 of LC3 and lysosome signals was calculated in young (n = 20), aged (n = 17), and Spd+aged (n = 17) M II oocytes. ****P < 0.0001, ****P < 0.0001. **c**, The MCC-M1 of VDAC1 and LC3 signals was calculated in young (n = 21), aged (n = 21), and Spd+aged (n = 17) M II oocytes. ***P = 0.0001, **P = 0.0046. **d**, The MCC-M2 of VDAC1 and LC3 signals was calculated in young (n = 21), aged (n = 21), and Spd+aged (n = 17) M II oocytes. ***P = 0.0003, *P = 0.0106. **e**, The MCC-M1 of mitochondrion and lysosome signals was calculated in young (n = 21), aged (n = 19), and Spd+aged (n = 16) M II oocytes. ****P < 0.0001, ****P < 0.0001. **f**, The MCC-M2 of mitochondrion and lysosome signals was calculated in young (n = 21), aged (n = 19), and Spd+aged (n = 16) M II oocytes. ****P < 0.0001, ****P < 0.0001. Data were presented as mean value (mean ± SD) of at least three independent experiments. Statistical significance was determined by two-tailed unpaired t-test.
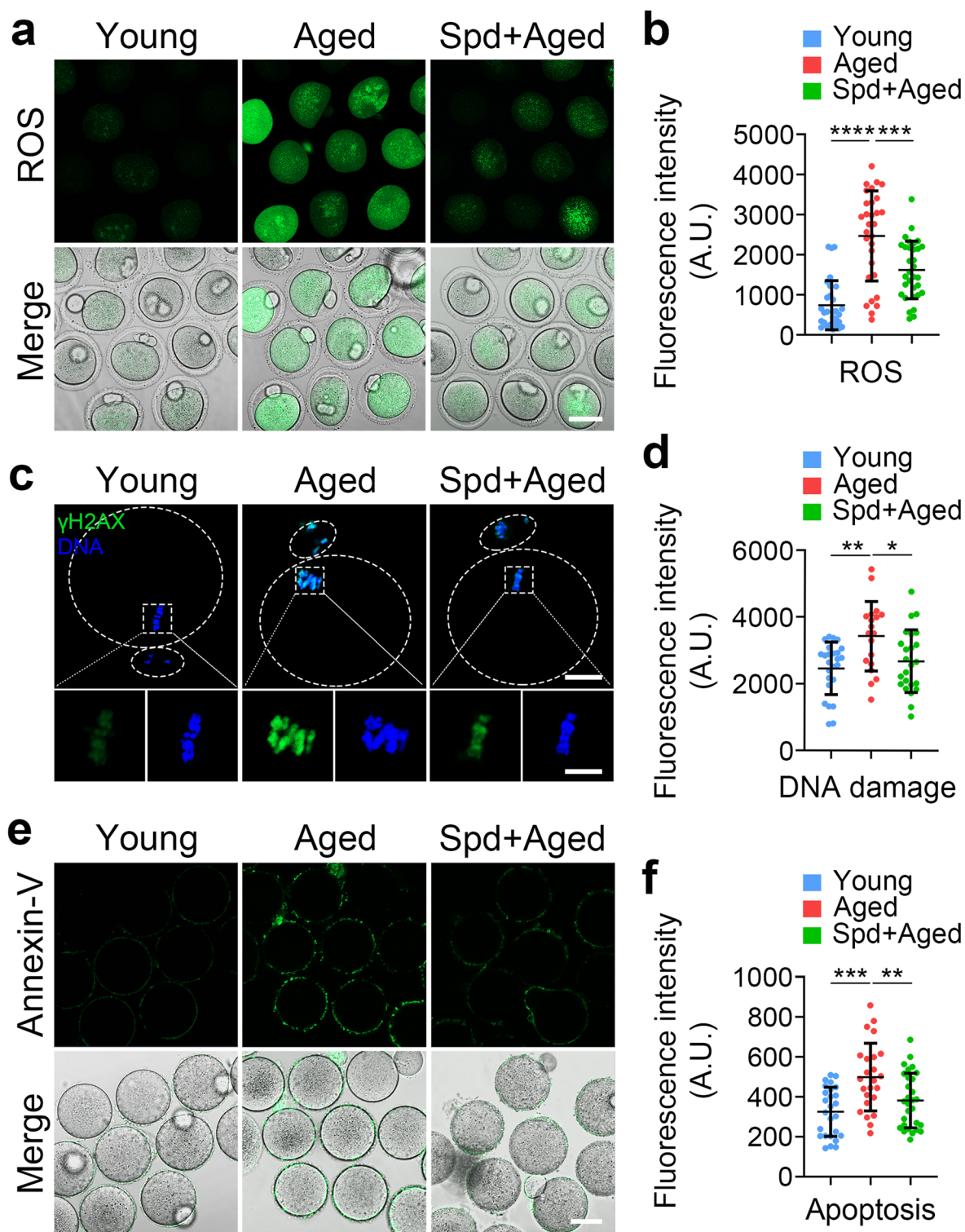
Extended Data Fig. 7 | Effects of spermidine supplementation on ROS levels, DNA damage accumulation and apoptosis in aged oocytes. a, Representative images of ROS levels as detected by DCFH staining in young, aged, and Spd+aged M II oocytes. Scale bar, 80 μm. **b**, The fluorescence intensity of ROS signals was measured in young (n = 30), aged (n = 30), and Spd+aged (n = 32) M II oocytes. ****P < 0.0001, ***P = 0.0007. **c**, Representative images of DNA damage as stained with γH2AX antibody in young, aged, and Spd+aged M II oocytes. Scale bar, 10 μm. **d**, The fluorescence intensity of γH2AX signals was quantified in

young (n = 25), aged (n = 19), and Spd+aged (n = 24) M II oocytes. **P = 0.0011, *P = 0.0175. **e**, Representative images of apoptotic oocytes at M II stage as assessed by Annexin-V staining in young, aged, and Spd+aged groups. Scale bar, 40 μm. **f**, The fluorescence intensity of Annexin-V signals was measured in young (n = 26), aged (n = 24), and Spd+aged (n = 29) M II oocytes. ***P = 0.0002, **P = 0.0074. Data in **b**, **d** and **f** were presented as mean value (mean ± SD) of at least three independent experiments. Statistical significance was determined by two-tailed unpaired t-test.

Extended Data Fig. 8 | See next page for caption.

Extended Data Fig. 8 | Effects of mitophagy inhibition on the improvement of aged oocytes by spermidine supplementation. a, The percentage of PB1 extrusion was quantified in control (n = 87) and Mdivi1-treated (10 μM: n = 88, 20 μM: n = 90, 50 μM: n = 98, 100 μM: n = 88, 150 μM: n = 64, 200 μM: n = 93) young oocytes after *in vitro* maturation for 14 h. P = 0.446, P = 0.1149, P = 0.059, **P = 0.003, ****P < 0.0001, ****P < 0.0001. **b**, Representative images of autophagosomes as stained with LC3 antibody in control and Mdivi-1-treated young M II oocytes. Scale bar, 40 μm. **c**, The fluorescence intensity of LC3 signals was measured in control (n = 28) and Mdivi-1-treated (10: n = 28, 20: n = 25, 50: n = 29, 100: n = 32, 150: n = 15) young M II oocytes. P = 0.6328, ****P < 0.0001, ****P < 0.0001, ****P < 0.0001, ****P < 0.0001. **d**, The percentage of PB1 extrusion was quantified in young (n = 94), aged (n = 83), Spd+aged (n = 67), and Spd+aged+Mdivi-1 (n = 86) oocytes after *in vitro* maturation for 14 h. **P = 0.0018, *P = 0.042, **P = 0.0041. **e**, Representative images of autophagosomes as stained with LC3 antibody in young, aged, Spd+aged, and Spd+aged+Mdivi-1 M II oocytes. Scale bar, 20 μm. **f**, The fluorescence intensity of LC3 signals was measured in young (n = 31), aged (n = 22), Spd+aged (n = 25), and Spd+aged+Mdivi-1 (n = 32) M II oocytes. ****P < 0.0001, **P = 0.0034, ***P = 0.0002. Data in **a**, **c**, **d** and **f** were presented as mean percentage (mean ± SEM) or mean value (mean ± SD) of at least three independent experiments. *P < 0.05; **P < 0.01; ***P < 0.001; ****P < 0.0001; ns, no significance. Statistical significance was determined by two-tailed unpaired *t*-test.
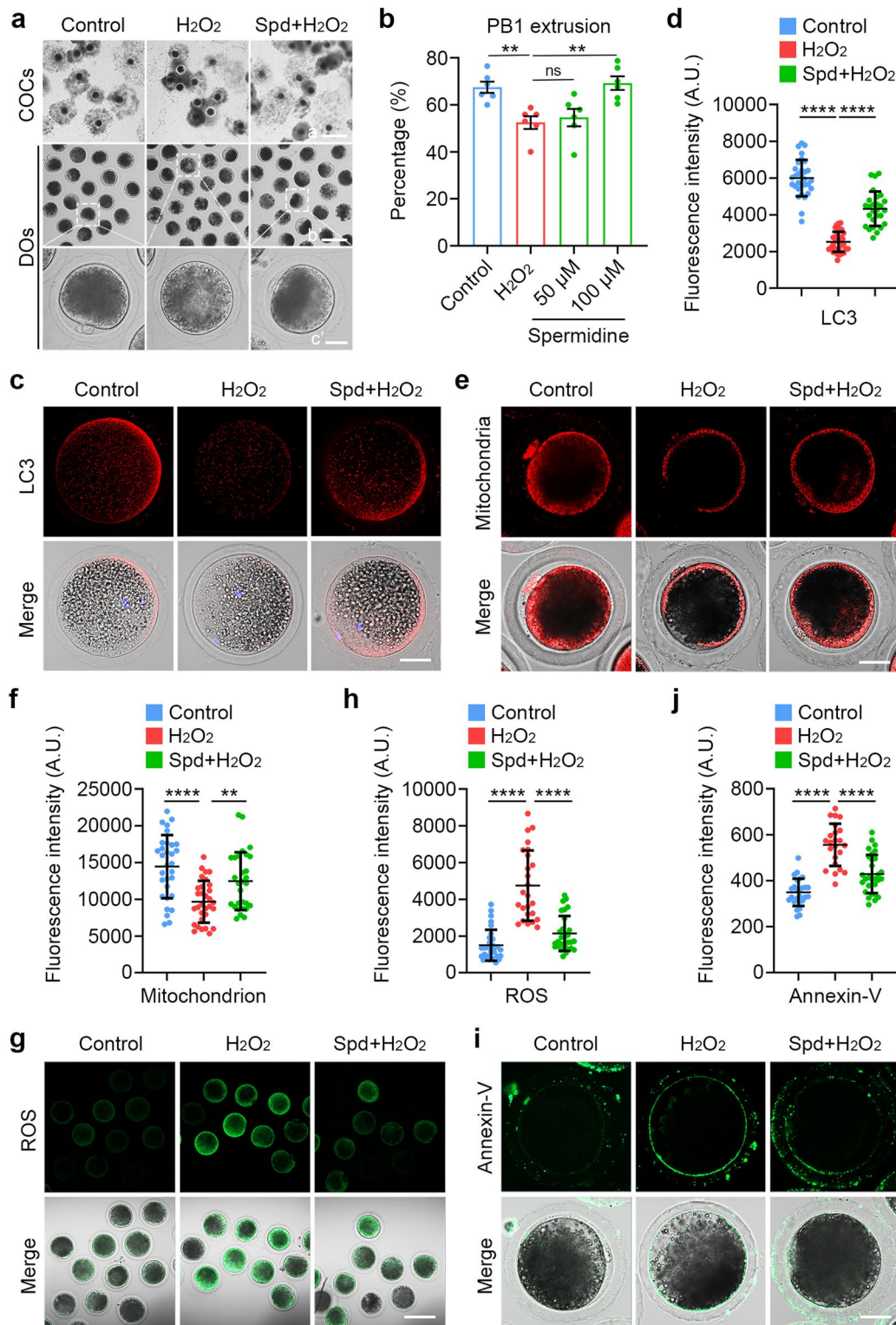
Extended Data Fig. 9 | See next page for caption.

Extended Data Fig. 9 | Effects of spermidine supplementation on the quality of porcine oocytes exposed to H2O2. a, Representative images of *in vitro* matured porcine oocytes in control, H_2O_2-treated, and Spd-supplemented groups. Scale bars: a', 400 μm; b', 200 μm; c', 40 μm. GV oocytes were treated with 100 μM H_2O_2 for 30 min and then cultured in the fresh medium with or without spermidine for *in vitro* maturation. **b**, The percentage of PB1 extrusion was recorded in control (n = 191), H_2O_2-treated (n = 203), and different concentrations of Spd-supplemented groups (50 μM: n = 196, 100 μM: n = 195) after *in vitro* culture for 44 h. **P = 0.002, P = 0.6526, **P = 0.0017. ns, no significance. **c**, Representative images of autophagosomes as stained with LC3 antibody in control, H_2O_2-treated, and Spd-supplemented oocytes at M II stage. Scale bar, 40 μm. **d**, The fluorescence intensity of LC3 signals was measured in control (n = 31), H_2O_2-treated (n = 36), and Spd-supplemented (n = 27) oocytes. ****P < 0.0001, ****P < 0.0001. **e**, Representative images of mitochondrial distribution in control, H_2O_2-treated, and Spd-supplemented oocytes. Scale bar, 40 μm. **f**, The fluorescence intensity of mitochondrial signals was measured in control (n = 31), H_2O_2-treated (n = 31), and Spd-supplemented (n = 29) oocytes. ****P < 0.0001, **P = 0.0023. **g**, Representative images of ROS levels detected by DCFH staining in control, H_2O_2-treated, and Spd-supplemented oocytes. Scale bar, 150 μm. **h**, The fluorescence intensity of ROS signals was measured in control (n = 30), H_2O_2-treated (n = 25), and Spd-supplemented (n = 31) oocytes. ****P < 0.0001, ****P < 0.0001. **i**, Representative images of apoptotic oocytes as assessed by Annexin-V staining in control, H_2O_2-treated, and Spd-supplemented groups. Scale bar, 40 μm. **j**, The fluorescence intensity of Annexin-V signals was measured in control (n = 26), H_2O_2-treated (n = 23), and Spd-supplemented (n = 30) oocytes. ****P < 0.0001, ****P < 0.0001. Data in **b**, **d**, **f**, **h** and **j** were presented as mean percentage or values (mean ± SEM or SD) of at least three independent experiments. Statistical significance was determined by two-tailed unpaired *t*-test.

nature portfolio

Corresponding author(s): Bo Xiong

Last updated by author(s): Jul 28, 2023

Reporting Summary

Nature Portfolio wishes to improve the reproducibility of the work that we publish. This form provides structure for consistency and transparency in reporting. For further information on Nature Portfolio policies, see our Editorial Policies and the Editorial Policy Checklist.

Statistics

For all statistical analyses, confirm that the following items are present in the figure legend, table legend, main text, or Methods section.

n/a	Confirmed	
☐	☒	The exact sample size (n) for each experimental group/condition, given as a discrete number and unit of measurement
☐	☒	A statement on whether measurements were taken from distinct samples or whether the same sample was measured repeatedly
☐	☒	The statistical test(s) used AND whether they are one- or two-sided *Only common tests should be described solely by name; describe more complex techniques in the Methods section.*
☒	☐	A description of all covariates tested
☐	☒	A description of any assumptions or corrections, such as tests of normality and adjustment for multiple comparisons
☐	☒	A full description of the statistical parameters including central tendency (e.g. means) or other basic estimates (e.g. regression coefficient) AND variation (e.g. standard deviation) or associated estimates of uncertainty (e.g. confidence intervals)
☐	☒	For null hypothesis testing, the test statistic (e.g. F, t, r) with confidence intervals, effect sizes, degrees of freedom and P value noted *Give P values as exact values whenever suitable.*
☒	☐	For Bayesian analysis, information on the choice of priors and Markov chain Monte Carlo settings
☒	☐	For hierarchical and complex designs, identification of the appropriate level for tests and full reporting of outcomes
☐	☒	Estimates of effect sizes (e.g. Cohen's d, Pearson's r), indicating how they were calculated

Our web collection on statistics for biologists contains articles on many of the points above.

Software and code

Policy information about availability of computer code

Data collection	Zeiss LSM software Zen 2.1 Blue QuantStudio Design & Analysis Software v1.4
Data analysis	GraphPad Prism 8 (8.2.1) (Fiji Is Just) ImageJ 2.1.0/1.53c Compound Discoverer 3.3 MetaX Bowtie2 v2.2.5 DESeq2 R (R Foundation for Statistical Computing, Vienna, Austria) SOAPnuke v1.5.2

For manuscripts utilizing custom algorithms or software that are central to the research but not yet described in published literature, software must be made available to editors and reviewers. We strongly encourage code deposition in a community repository (e.g. GitHub). See the Nature Portfolio guidelines for submitting code & software for further information.

Data

Policy information about availability of data

All manuscripts must include a data availability statement. This statement should provide the following information, where applicable:

- Accession codes, unique identifiers, or web links for publicly available datasets
- A description of any restrictions on data availability
- For clinical datasets or third party data, please ensure that the statement adheres to our policy

> Transcriptomic raw data have been deposited in Gene Expression Omnibus (GEO) database under accession number GSE239551. Source data are provided with this paper.

Human research participants

Policy information about studies involving human research participants and Sex and Gender in Research.

Reporting on sex and gender	*Use the terms sex (biological attribute) and gender (shaped by social and cultural circumstances) carefully in order to avoid confusing both terms. Indicate if findings apply to only one sex or gender; describe whether sex and gender were considered in study design whether sex and/or gender was determined based on self-reporting or assigned and methods used. Provide in the source data disaggregated sex and gender data where this information has been collected, and consent has been obtained for sharing of individual-level data; provide overall numbers in this Reporting Summary. Please state if this information has not been collected. Report sex- and gender-based analyses where performed, justify reasons for lack of sex- and gender-based analysis.*
Population characteristics	*Describe the covariate-relevant population characteristics of the human research participants (e.g. age, genotypic information, past and current diagnosis and treatment categories). If you filled out the behavioural & social sciences study design questions and have nothing to add here, write "See above."*
Recruitment	*Describe how participants were recruited. Outline any potential self-selection bias or other biases that may be present and how these are likely to impact results.*
Ethics oversight	*Identify the organization(s) that approved the study protocol.*

Note that full information on the approval of the study protocol must also be provided in the manuscript.

Field-specific reporting

Please select the one below that is the best fit for your research. If you are not sure, read the appropriate sections before making your selection.

☒ Life sciences   ☐ Behavioural & social sciences   ☐ Ecological, evolutionary & environmental sciences

For a reference copy of the document with all sections, see nature.com/documents/nr-reporting-summary-flat.pdf

Life sciences study design

All studies must disclose on these points even when the disclosure is negative.

Sample size	No statistical methods were used to pre-determine sample sizes. Sample sizes were determined based on our previous studies (Zhou et al., Science Advances, 2021; Miao et al., Cell Reports, 2020; Zhou et al., Science Advances, 2020).
Data exclusions	No data were excluded from the analyses.
Replication	All experiments were independently repeated at least three times unless otherwise stated.
Randomization	No randomization methods were used.
Blinding	Data collection and statistical analyses were not analyzed blinded to the experimental conditions.

Reporting for specific materials, systems and methods

We require information from authors about some types of materials, experimental systems and methods used in many studies. Here, indicate whether each material, system or method listed is relevant to your study. If you are not sure if a list item applies to your research, read the appropriate section before selecting a response.

Materials & experimental systems

n/a	Involved in the study
☐ ☒	Antibodies
☐ ☐	Eukaryotic cell lines
☐ ☐	Palaeontology and archaeology
☐ ☒	Animals and other organisms
☐ ☐	Clinical data
☐ ☐	Dual use research of concern

Methods

n/a	Involved in the study
☐ ☐	ChIP-seq
☐ ☐	Flow cytometry
☐ ☐	MRI-based neuroimaging

Antibodies

Antibodies used	Mouse monoclonal anti-α-tubulin-FITC , Sigma-Aldrich, F2168, 1:200 Rabbit monoclonal anti-γH2AX, Cell Signaling Technology, 9718, 1:100 Rabbit polyclonal anti-microtubule associated protein 1 light chain 3B (LC3B), Cell Signaling Technology, 2775, 1:100 Human anti-centromere, Antibodies Incorporated, 15-234, 1:200 Mouse monoclonal anti-ASTL, Santa Cruz Biotechnology, sc-514054, 1:100 Rabbit monoclonal anti-VDAC1, ABclonal Technology, A19707, 1:100
Validation	All antibodies were commercially available. Antibody clones were selected based on validation data shown on the manufacturer's website.

Eukaryotic cell lines

Policy information about cell lines and Sex and Gender in Research

Cell line source(s)	State the source of each cell line used and the sex of all primary cell lines and cells derived from human participants or vertebrate models.
Authentication	Describe the authentication procedures for each cell line used OR declare that none of the cell lines used were authenticated.
Mycoplasma contamination	Confirm that all cell lines tested negative for mycoplasma contamination OR describe the results of the testing for mycoplasma contamination OR declare that the cell lines were not tested for mycoplasma contamination.
Commonly misidentified lines (See ICLAC register)	Name any commonly misidentified cell lines used in the study and provide a rationale for their use.

Palaeontology and Archaeology

Specimen provenance	Provide provenance information for specimens and describe permits that were obtained for the work (including the name of the issuing authority, the date of issue, and any identifying information). Permits should encompass collection and, where applicable, export.
Specimen deposition	Indicate where the specimens have been deposited to permit free access by other researchers.
Dating methods	If new dates are provided, describe how they were obtained (e.g. collection, storage, sample pretreatment and measurement), where they were obtained (i.e. lab name), the calibration program and the protocol for quality assurance OR state that no new dates are provided.

☐ Tick this box to confirm that the raw and calibrated dates are available in the paper or in Supplementary Information.

Ethics oversight	Identify the organization(s) that approved or provided guidance on the study protocol, OR state that no ethical approval or guidance was required and explain why not.

Note that full information on the approval of the study protocol must also be provided in the manuscript.

Animals and other research organisms

Policy information about studies involving animals; ARRIVE guidelines recommended for reporting animal research, and Sex and Gender in Research

Laboratory animals	The young (6~8 week old) and aged (52~56 week old) ICR female mice were housed in a 12 h light-dark cycle with constant temperature and free access to food and water. Aged mice were intraperitoneally injected daily with spermidine (Sigma-Aldrich; 50 mg/kg body weight per day, dissolved in PBS) or the equivalent volume of PBS according to previous studies for 10 consecutive days. Or, aged mice were supplemented with spermidine at 3 mM in drinking water as previously reported for 30 days.

Wild animals	No wild animals were used for this study.
Reporting on sex	*Indicate if findings apply to only one sex; describe whether sex was considered in study design, methods used for assigning sex. Provide data disaggregated for sex where this information has been collected in the source data as appropriate; provide overall numbers in this Reporting Summary. Please state if this information has not been collected. Report sex-based analyses where performed, justify reasons for lack of sex-based analysis.*
Field-collected samples	This study did not involve samples collected in the field.
Ethics oversight	All animal studies were authorized and approved by the Animal Research Institute Committee of Nanjing Agricultural University.

Note that full information on the approval of the study protocol must also be provided in the manuscript.

Clinical data

Policy information about clinical studies

All manuscripts should comply with the ICMJE guidelines for publication of clinical research and a completed CONSORT checklist must be included with all submissions.

Clinical trial registration	*Provide the trial registration number from ClinicalTrials.gov or an equivalent agency.*
Study protocol	*Note where the full trial protocol can be accessed OR if not available, explain why.*
Data collection	*Describe the settings and locales of data collection, noting the time periods of recruitment and data collection.*
Outcomes	*Describe how you pre-defined primary and secondary outcome measures and how you assessed these measures.*

Dual use research of concern

Policy information about dual use research of concern

Hazards

Could the accidental, deliberate or reckless misuse of agents or technologies generated in the work, or the application of information presented in the manuscript, pose a threat to:

No | Yes
☐ ☐ Public health
☐ ☐ National security
☐ ☐ Crops and/or livestock
☐ ☐ Ecosystems
☐ ☐ Any other significant area

Experiments of concern

Does the work involve any of these experiments of concern:

No | Yes
☐ ☐ Demonstrate how to render a vaccine ineffective
☐ ☐ Confer resistance to therapeutically useful antibiotics or antiviral agents
☐ ☐ Enhance the virulence of a pathogen or render a nonpathogen virulent
☐ ☐ Increase transmissibility of a pathogen
☐ ☐ Alter the host range of a pathogen
☐ ☐ Enable evasion of diagnostic/detection modalities
☐ ☐ Enable the weaponization of a biological agent or toxin
☐ ☐ Any other potentially harmful combination of experiments and agents

ChIP-seq

Data deposition

☐ Confirm that both raw and final processed data have been deposited in a public database such as GEO.

☐ Confirm that you have deposited or provided access to graph files (e.g. BED files) for the called peaks.

| Data access links | *For "Initial submission" or "Revised version" documents, provide reviewer access links. For your "Final submission" document,* |

Data access links	*provide a link to the deposited data.*
Files in database submission	*Provide a list of all files available in the database submission.*
Genome browser session (e.g. UCSC)	*Provide a link to an anonymized genome browser session for "Initial submission" and "Revised version" documents only, to enable peer review. Write "no longer applicable" for "Final submission" documents.*

Methodology

Replicates	*Describe the experimental replicates, specifying number, type and replicate agreement.*
Sequencing depth	*Describe the sequencing depth for each experiment, providing the total number of reads, uniquely mapped reads, length of reads and whether they were paired- or single-end.*
Antibodies	*Describe the antibodies used for the ChIP-seq experiments; as applicable, provide supplier name, catalog number, clone name, and lot number.*
Peak calling parameters	*Specify the command line program and parameters used for read mapping and peak calling, including the ChIP, control and index files used.*
Data quality	*Describe the methods used to ensure data quality in full detail, including how many peaks are at FDR 5% and above 5-fold enrichment.*
Software	*Describe the software used to collect and analyze the ChIP-seq data. For custom code that has been deposited into a community repository, provide accession details.*

Flow Cytometry

Plots

Confirm that:

☐ The axis labels state the marker and fluorochrome used (e.g. CD4-FITC).

☐ The axis scales are clearly visible. Include numbers along axes only for bottom left plot of group (a 'group' is an analysis of identical markers).

☐ All plots are contour plots with outliers or pseudocolor plots.

☐ A numerical value for number of cells or percentage (with statistics) is provided.

Methodology

Sample preparation	*Describe the sample preparation, detailing the biological source of the cells and any tissue processing steps used.*
Instrument	*Identify the instrument used for data collection, specifying make and model number.*
Software	*Describe the software used to collect and analyze the flow cytometry data. For custom code that has been deposited into a community repository, provide accession details.*
Cell population abundance	*Describe the abundance of the relevant cell populations within post-sort fractions, providing details on the purity of the samples and how it was determined.*
Gating strategy	*Describe the gating strategy used for all relevant experiments, specifying the preliminary FSC/SSC gates of the starting cell population, indicating where boundaries between "positive" and "negative" staining cell populations are defined.*

☐ Tick this box to confirm that a figure exemplifying the gating strategy is provided in the Supplementary Information.

Magnetic resonance imaging

Experimental design

Design type	*Indicate task or resting state; event-related or block design.*
Design specifications	*Specify the number of blocks, trials or experimental units per session and/or subject, and specify the length of each trial or block (if trials are blocked) and interval between trials.*
Behavioral performance measures	*State number and/or type of variables recorded (e.g. correct button press, response time) and what statistics were used to establish that the subjects were performing the task as expected (e.g. mean, range, and/or standard deviation across subjects).*

Acquisition

Imaging type(s)
Specify: functional, structural, diffusion, perfusion.

Field strength
Specify in Tesla

Sequence & imaging parameters
Specify the pulse sequence type (gradient echo, spin echo, etc.), imaging type (EPI, spiral, etc.), field of view, matrix size, slice thickness, orientation and TE/TR/flip angle.

Area of acquisition
State whether a whole brain scan was used OR define the area of acquisition, describing how the region was determined.

Diffusion MRI ☐ Used ☐ Not used

Preprocessing

Preprocessing software
Provide detail on software version and revision number and on specific parameters (model/functions, brain extraction, segmentation, smoothing kernel size, etc.).

Normalization
If data were normalized/standardized, describe the approach(es): specify linear or non-linear and define image types used for transformation OR indicate that data were not normalized and explain rationale for lack of normalization.

Normalization template
Describe the template used for normalization/transformation, specifying subject space or group standardized space (e.g. original Talairach, MNI305, ICBM152) OR indicate that the data were not normalized.

Noise and artifact removal
Describe your procedure(s) for artifact and structured noise removal, specifying motion parameters, tissue signals and physiological signals (heart rate, respiration).

Volume censoring
Define your software and/or method and criteria for volume censoring, and state the extent of such censoring.

Statistical modeling & inference

Model type and settings
Specify type (mass univariate, multivariate, RSA, predictive, etc.) and describe essential details of the model at the first and second levels (e.g. fixed, random or mixed effects; drift or auto-correlation).

Effect(s) tested
Define precise effect in terms of the task or stimulus conditions instead of psychological concepts and indicate whether ANOVA or factorial designs were used.

Specify type of analysis: ☐ Whole brain ☐ ROI-based ☐ Both

Statistic type for inference
(See Eklund et al. 2016)
Specify voxel-wise or cluster-wise and report all relevant parameters for cluster-wise methods.

Correction
Describe the type of correction and how it is obtained for multiple comparisons (e.g. FWE, FDR, permutation or Monte Carlo).

Models & analysis

n/a | Involved in the study
☐ | ☐ Functional and/or effective connectivity
☐ | ☐ Graph analysis
☐ | ☐ Multivariate modeling or predictive analysis

Functional and/or effective connectivity
Report the measures of dependence used and the model details (e.g. Pearson correlation, partial correlation, mutual information).

Graph analysis
Report the dependent variable and connectivity measure, specifying weighted graph or binarized graph, subject- or group-level, and the global and/or node summaries used (e.g. clustering coefficient, efficiency, etc.).

Multivariate modeling and predictive analysis
Specify independent variables, features extraction and dimension reduction, model, training and evaluation metrics.